This is to certify that the

dissertation entitled

THE EFFECTS OF SR^{2+}-SUBSTITUTION ON THE REDUCTION RATES OF $Yz^{\bullet}$ AND ON THE HYDROGEN ATOM ABSTRACTION MECHANISM IN PHOTOSYSTEM II

presented by

Kristi L. Westphal

has been accepted towards fulfillment
of the requirements for

Ph.D. degree in Chemistry

G. T. Babcock

Major professor

Date Aug 11, 2000

THE EFFECTS OF SR^{2+}-SUBSTITUTION ON THE REDUCTION RATES OF $Y_Z^{\bullet}$ AND ON THE HYDROGEN ATOM ABSTRACTION MECHANISM IN PHOTOSYSTEM II

By

Kristi L. Westphal

A DISSERTATION

Submitted to
Michigan State University
in partial fulfillment of the requirements
for the degree of

DOCTOR OF PHILOSOPHY

Department of Chemistry

2000

ABSTRACT

THE EFFECTS OF SR^{2+}-SUBSTITUTION ON THE REDUCTION RATES OF $Y_Z^{\bullet}$ AND ON THE HYDROGEN ATOM ABSTRACTION MECHANISM IN PHOTOSYTEM II

By

Kristi L. Westphal

Photosystem II is a photosynthetic enzyme that catalyzes the light-driven oxidation of water to molecular oxygen. A total of four sequential light-induced turnovers of Photosystem II are required to form molecular oxygen. Each stable intermediate produced by a flash of light is called an S_n-state, n = 0-4. A general consensus has not yet been reached concerning the mechanism of this reaction or the structure of Photosystem II, although much progress has been made over the last few years. It is generally agreed upon that the oxygen-evolving complex of Photosystem II consists of a manganese cluster made up of four manganese atoms, a redox-active tyrosine called Y_z, histidine 190, and Ca^{2+} and Cl^- ions. Recently, several models have been proposed that directly involve Y_z in the water oxidation chemistry as a hydrogen atom abstractor. Perhaps the most elusive subject is the role of Ca^{2+} in PSII. Two main proposals have been set forth: 1) Ca^{2+} plays a structural role and a binding site for Cl^- and, 2) Ca^{2+} is

directly involved in the oxygen-oxygen bond forming reaction. One way to acquire more information on the role of Ca^{2+} is to perform biochemical treatments that perturb this cofactor and then monitor the kinetic efficiency of the oxygen-evolving complex.

Several groups have recently investigated the effects of biochemical treatments, site-directed mutagenesis, or substitution of essential cofactors on the kinetics of the stepwise, water-oxidizing chemistry catalyzed by Photosystem II. Consistently, these studies showed evidence for a slowing of the final, oxygen-releasing step, $S_3 \rightarrow S_0$, of the catalytic cycle. To a degree, some of this work also showed a slowing of the earlier S-state transitions. To test the roles that have been proposed for Ca^{2+}, PSII membranes were depleted of Ca^{2+} and subsequently reconstitution with Sr^{2+}. The rates of the S-state transitions in these samples were monitored by using time-resolved electron paramagnetic resonance spectroscopy. The results show a slowdown of the last transition in the cycle, consistent with an earlier report from Boussac and Rutherford (Boussac, A., Setif, P. and Rutherford, A.W. (1992) *Biochemistry 31*, 1224-1234), and of the earlier S-state transitions as well. Our observations that both the lower and higher S-state transition rates decrease suggest that a common molecular mechanism is at work and that Sr^{2+} is less effective than Ca^{2+} in supporting it.

The time-resolved electron paramagnetic resonance spectroscopy results were also analyzed in the context of the hydrogen atom abstraction mechanism. The retarding effect caused by Sr^{2+} substitution is additional evidence to support

this mechanism. Furthermore, the hydrogen atom abstraction mechanism is best able to explain the unusual characteristics of the S-state transitions: slow rates, low activation energies, low pre-exponential factors, and small kinetic isotope effects.

In Memory of My Father, Bruce G. Westphal

ACKNOWLEDGMENTS

I would like to begin by thanking my research advisor, Jerry Babcock, for his guidance, patience, and support. I couldn't have asked for a better advisor!

I would like to thank my mother, Diana Westphal, for her words of encouragement when I needed them most and for her never-ending faith in my becoming Dr. Westphal.

I would also like to thank my boyfriend, Marcus Sims, for putting up with me when I knew I was unbearable to be around and for always being able to make me laugh! Also, for his words of encouragement when I was pulling my hair out in frustration (especially writing this thing!).

I would lastly like to thank my lab mates and friends for being there when I needed help or just needed a good laugh (some of you probably didn't even know you were supplying the latter!) I would particularly like to thank three of these people. First, my partner in crime, Heather Sackett, without you I would have had no one to talk stupid with or to surf the net for questionable web sites! Second, my second partner in crime and softball buddie, Shannon Haymond, may we never have another wine night like the first! Thirdly, Hans Schelvis, my desk neighbor for the past five years. You were always there to answer my questions and to make the best coffee! I will miss you all dearly.

Thanks to everyone who have made my graduate school experience one that I will never forget!

TABLE OF CONTENTS

LIST OF TABLES

LIST OF FIGURES

Chapter 1

1 Introduction

Two to three billion years ago photosynthetic cyanobacteria gained the capability to extract electrons from water and produce molecular oxygen as a byproduct. These organisms flourished on an inexhaustible supply of water, transforming the earth's atmosphere from a composition of reduced gases to one rich in O_2. Prior to this event, all organisms on earth were adapted to an anaerobic environment. As the atmosphere became enriched in oxygen, many organisms became extinct while the others adapted to the new environment. As a consequence, the highly efficient process of respiration evolved and higher organisms developed. Today, members of the higher plants, algae, and cyanobacteria families are all capable of carrying out oxygenic photosynthesis.

1.1 The Electron Transport Chain in Photosynthesis

Photosynthesis in green plants is carried out by two photosystems, Photosystem I (PSI) and Photosystem II (PSII) which undergo photochemical charge separation. The two photosystems are located in the stromal region of the chloroplast in membranous structures called thylakoids, which are located within the leaf of the plant. Two additional membranous components are also involved in the electron transport chain: the cytochrome b_6f complex (cyt b_6f) and adenosine 5'-triphosphate (ATP) synthase. The flow of electrons through these components is illustrated in Figure 1.1 and is initiated by a light-induced charge separation in PSII, which takes electrons from water and delivers them to the mobile electron carrier plastoquinone (PQ). Next, PQ travels to cyt b_6f, which is

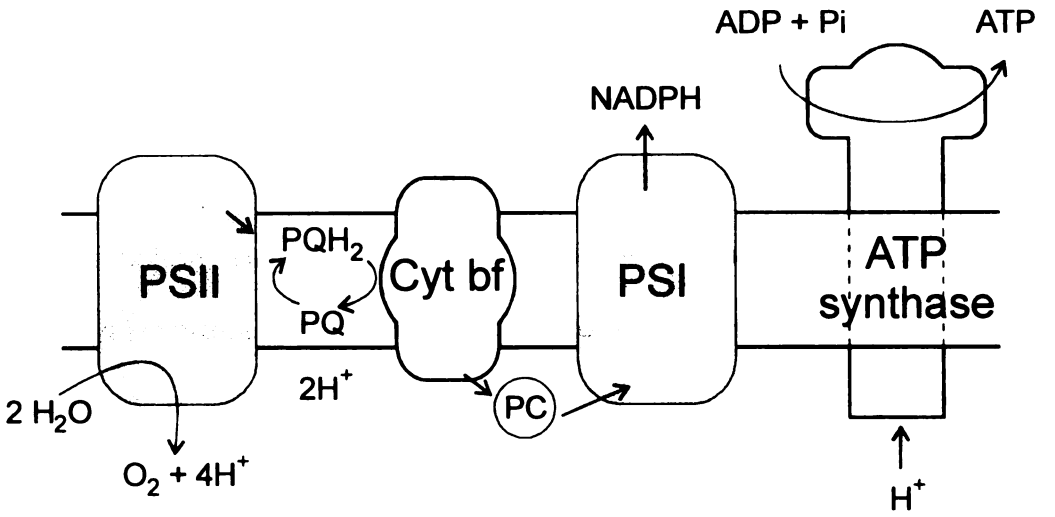

Figure 1-1 Flow of electrons through the electron transport chain in higher plants. This figure was kindly provided by Warwick Hillier.

involved in proton translocation, and then the electrons are taken up by a second mobile electron carrier called plastocyanin (PC) which delivers the electrons to PSI. Here the electrons are utilized in the terminal step of the electron transport chain where a molecule of nicotinamide adenine dinucleotide phosphate ($NADP^+$) is reduced to NADPH. In addition to the utilization of electrons for NADPH production, electron flow within each photosystem and between them induces a membrane potential through the translocation of protons. The electrochemical potential produced is then dissipated by ATP synthase in the production of ATP. The photosynthetic end products, NADPH and ATP, are both ultimately used by the plant to drive the synthesis of complex biomolecules essential for growth and reproduction.

1.2 Photosystem II

1.2.1 Polypeptide Composition and Electron Transfer Reactions

The photochemistry of PSII is performed on a protein scaffold that binds pigments and cofactors involved in the reaction. A schematic representation of the primary photochemical events that occur at PSII is depicted in Figure 1-2 (for reviews see (*1, 2*)). Light is first absorbed by the light-harvesting complex located peripherally to the PSII core, which consists of non-covalently bound pigment molecules including chlorophyll *a*, chlorophyll *b* and carotenoids (not shown in figure). The absorbed photon is then funneled into the reaction center to a specialized chlorophyll complex referred to as P_{680}. Excitation of P_{680} results in formation of the radical pair, $P_{680}^{\bullet+}Pheo^{\bullet-}$, which is stabilized by rapid electron

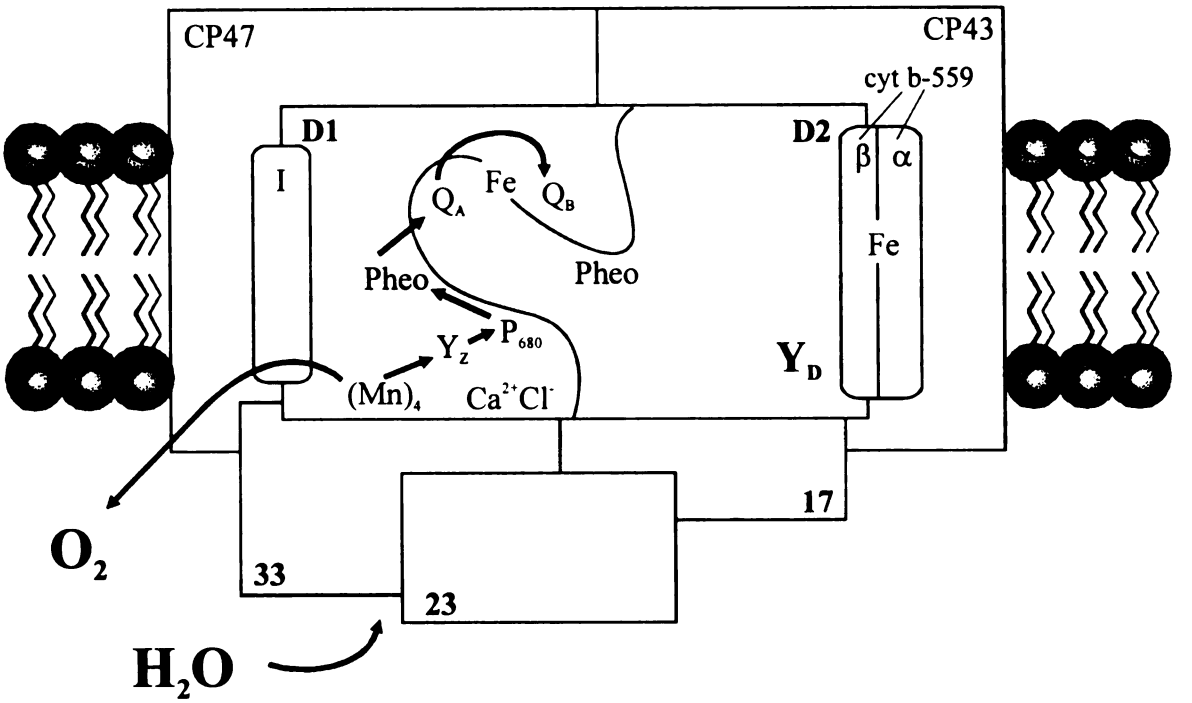

Figure 1-2 Schematic representation of the major polypeptides and redox components of PSII. The arrows show the flow of electrons.

transfer to a bound plastoquinone molecule, Q_A. A second plastoquinone molecule, Q_B, oxidizes Q_A^- within 100-200 μs, and after an additional charge-separation and subsequent protonation, the Q_BH_2 plastoquinol (PQ) formed leaves the reaction center and is replaced by an oxidized quinone from the plastoquinone pool. The electron hole that is produced at P_{680} is quickly reduced in nanoseconds by a redox-active tryosine residue, Y_z at D1-161. Subsequently, Y_z is reduced on the microsecond to millisecond time-scale by a Mn cluster consisting of four Mn atoms. The $(Mn)_4$ cluster and Y_z, along with the necessary cofactors Ca^{2+} and Cl^-, make up what is called the oxygen-evolving complex (OEC) of PSII, and it is at this site where the oxidation of water is catalyzed.

In *vivo*, PSII contains at least 20 polypeptides, but the minimal oxygen-evolving complex consists of seven major polypeptides: D1, D2, CP43, CP47, the α and β polypeptides of cyt *b*-559, and the extrinsic polypeptide of 33 kDa (for a recent review see (*3*)). The D1 and D2 polypeptides, which each contain five transmembrane helices, form the photochemical reaction center by binding P_{680}, Pheo, the non-heme iron, Q_A, Q_B, and contain the tyrosine Y_z, as well as a second redox active tyrosine referred to as Y_D. Both the D1 and D2 proteins exhibit a very high degree of sequence homology and appear to form a heterodimer with C_2 symmetry. It is estimated that there are 6 chlorophyll *a* molecules and 2 *β*-carotene molecules per D1/D2 reaction center. An oxygen-evolving reaction center requires, in addition to D1 and D2, two other chlorophyll-containing polypeptides known as CP47 and CP43. Both peptides contain about 15 bound chlorophyll *a* molecules and 2-3 molecules of β-carotene; they are

believed to act as inner antennae that transfer energy from the light-harvesting complex to the reaction center P_{680}. Cytochrome *b*-559, another necessary component of PSII, consists of two smaller polypeptides known as the α and β polypeptides, and has been proposed to protect PSII from photooxidative damage. The seventh major polypeptide of PSII has a molecular weight of 33 kDa and is located extrinsically to PSII. It is referred to as the manganese stabilizing protein (MSP) because it acts to protect the $(Mn)_4$ complex from exogenous reductants and optimizes the complex's catalytic efficiency. Two other extrinsic polypeptides are associated with PSII and have molecular weights of 17 and 23 kDa. They are implicated in the efficient production of oxygen by acting as barriers that prevent Ca^{2+} from migrating out of the site. Besides the major polypeptides described above, there are several small peptides associated with functional PSII complexes whose exact roles are unknown.

1.2.2 S-state Cycle in Water Oxidation

One of the first ground-breaking experiments in understanding water oxidation was performed in 1969 by Joliot and coworkers who studied oxygen yields from dark-adapted chloroplasts as a function of single-turnover flashes (*4*). This work, shown in Figure 1-3, demonstrated that after the third flash and every fourth flash thereafter, a maximum in oxygen yield occurs. This pattern of oxygen release indicated that a total of four sequential light-induced turnovers of PSII are required to form molecular oxygen. Shortly after, Kok and coworkers interpreted these results by formulating a kinetic model where each stable intermediate produced by a flash of light is called an S-state (*5*). Each S-state is designated

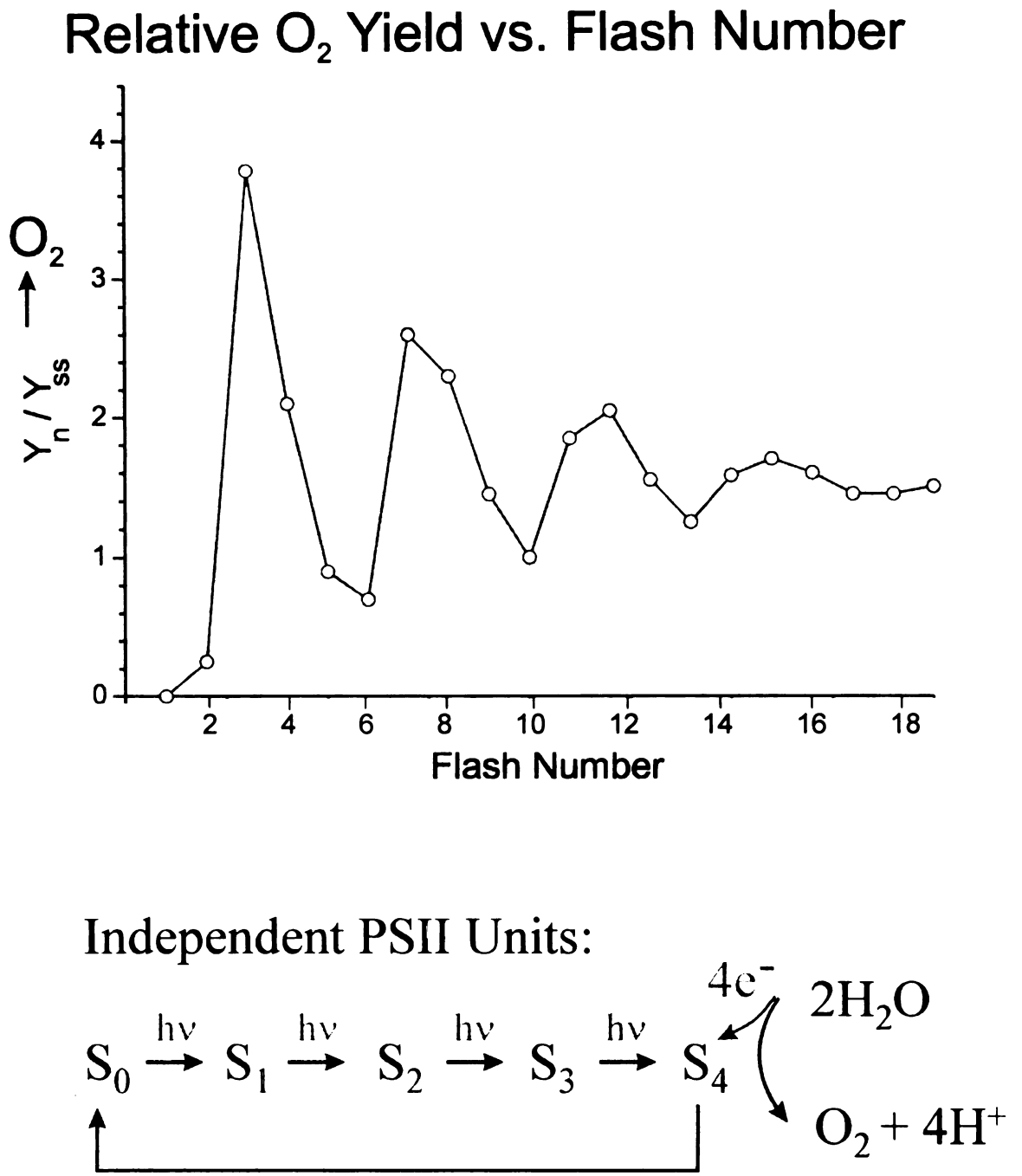

Figure 1-3 A period-four oscillation of oxygen evolution as a function of flash number in spinach chloroplasts. This figure was kindly provided by Gerald T. Babcock.

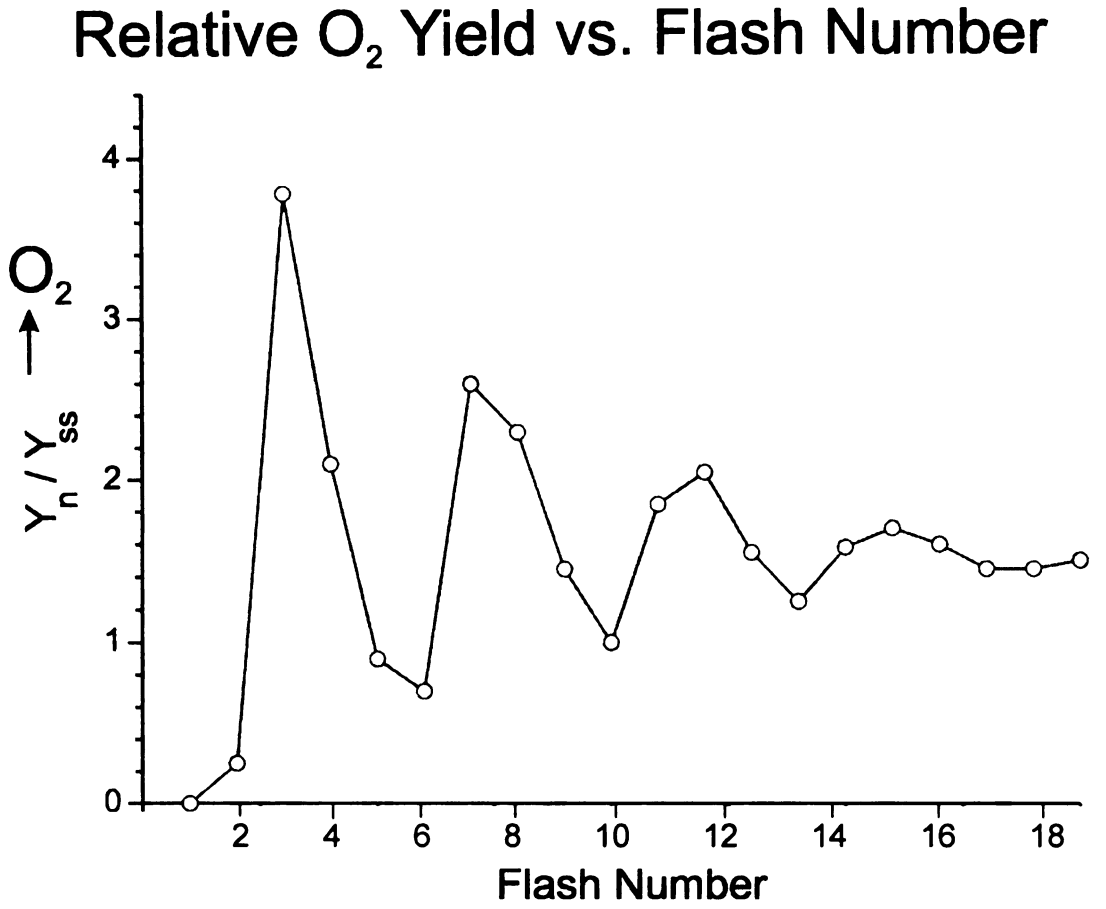

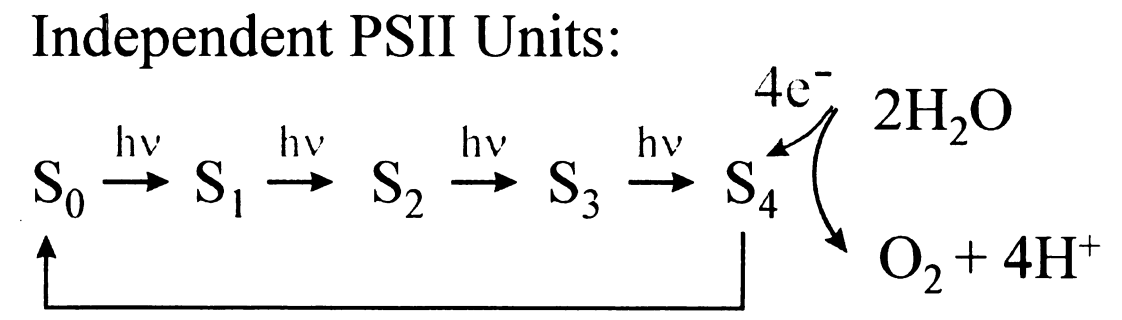

Figure 1-3 A period-four oscillation of oxygen evolution as a function of flash number in spinach chloroplasts. This figure was kindly provided by Gerald T. Babcock.

by S_n, where *n* is the number of oxidizing equivalents stored in the OEC. The S_1 state predominates in dark-adapted samples and the S_4 state is a transient intermediate that spontaneously reverts to the S_0 state with the concomitant release of O_2.

1.2.3 The Energetics of Water Oxidation

Water is an extremely stable molecule as evidenced by the fact that it covers over 75% of the earth's surface. Thus, in order to oxidize water to molecular oxygen very high reduction potentials are required. P_{680}^+, a product of the initial charge-separation reaction of PSII, is one of the strongest oxidants known in biology (*6*) and is sufficient enough to oxidize water (*7*). Figure 1-4 shows the reduction potentials of the major components of the donor and acceptor sides of PSII. A total of 3.72 V must be accumulated by the OEC in order to oxidize water (*8*). With a reduction potential of about 1.12 V, P_{680}^+ oxidizes Y_z, which has a reduction potential of about 0.97 V. Therefore, about 4 V of energy is supplied by PSII to oxidize water, which leaves little surplus energy available to support any potential fluctuations as the OEC proceeds through the S-state cycle. This weak coupling of the cofactors leads to the highly efficient conversion of about two thirds of the photon energy into chemical potential (*9-11*).

1.2.4 The Manganese Cluster

The PSII complex contains four manganese atoms per P_{680}. From extended X-ray absorption fine structure (EXAFS) measurements, a model was

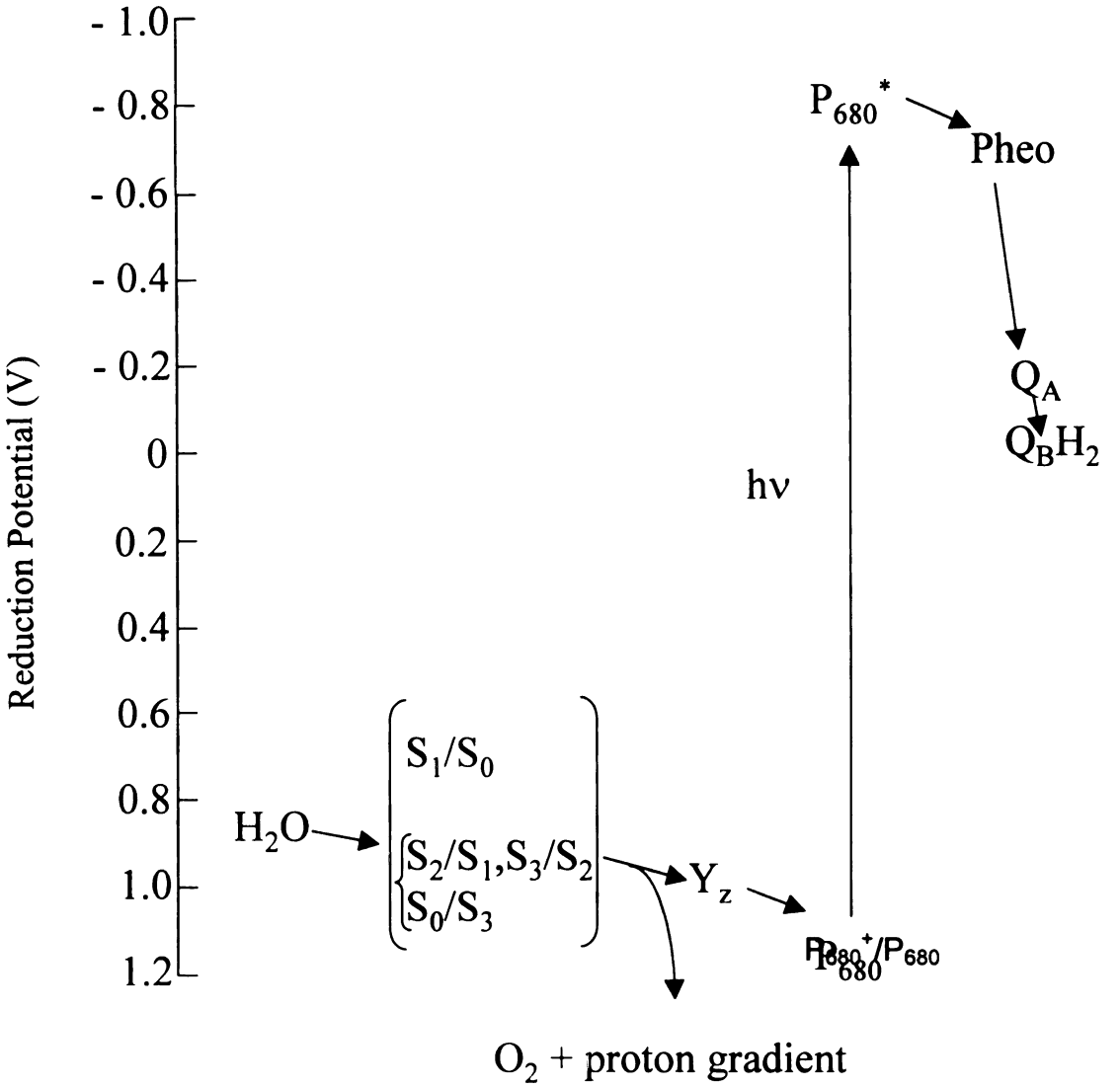

Figure 1-4 Redox potentials of the cofactors of PSII.

suggested for the local structure of the Mn complex. The model was proposed to consist of a pair of μ-oxo bridged dimers with Mn-Mn distances of 2.7 Å linked together by a mono-μ-oxo bridge with a Mn-Mn separation of 3.3 Å arranged in a C-shaped structure (*12, 13*). There are two well-established low temperature EPR signals refered to as the multiline and the g = 4.1 signals that have been attributed to the S_2 state of the $(Mn)_4$ cluster (*14, 15*). The multiline signal, shown in Figure 1-5 (b), displays 18-20 partially resolved hyperfine lines and has a linewidth of about 1500-1800 G. The signal is generated by illumination of O_2-evolving PSII samples at 160-200 K (Dismukes, 1980 #211; Hansson, 1982 #180; Brudvig, 1983 #179). Two other forms of the multiline signal can be generated by either Ca^{2+}-depletion (*16-18*) or ammonia treatment (*19-21*) of PSII samples. Both treatments affect the number and splittings of the hyperfine lines, and have therefore been proposed to directly affect the structure of the $(Mn)_4$ cluster.

The g = 4.1 signal, shown in Figure 1-5 (a), is due to a high-spin, ground state of the $(Mn)_4$ cluster (*22*) and is generated by illumination of PSII samples at 140 K in the presence of high concentrations of cryoprotectant (*15, 23*). This signal has a linewidth of 320-360 G and lacks resolved hyperfine structure. Upon warming in the dark, the g = 4.1 signal converts to the multiline signal.

Inhibition of PSII samples by incubation with acetate, which causes perturbations in the Ca^{2+} and Cl^- sites, traps the OEC in a state in which the EPR spectrum from $Y_z^{\bullet}$ is split by a magnetic interaction with the manganese S_2 state. This split EPR signal was first discovered by Rutherford and co-workers (*24*) and

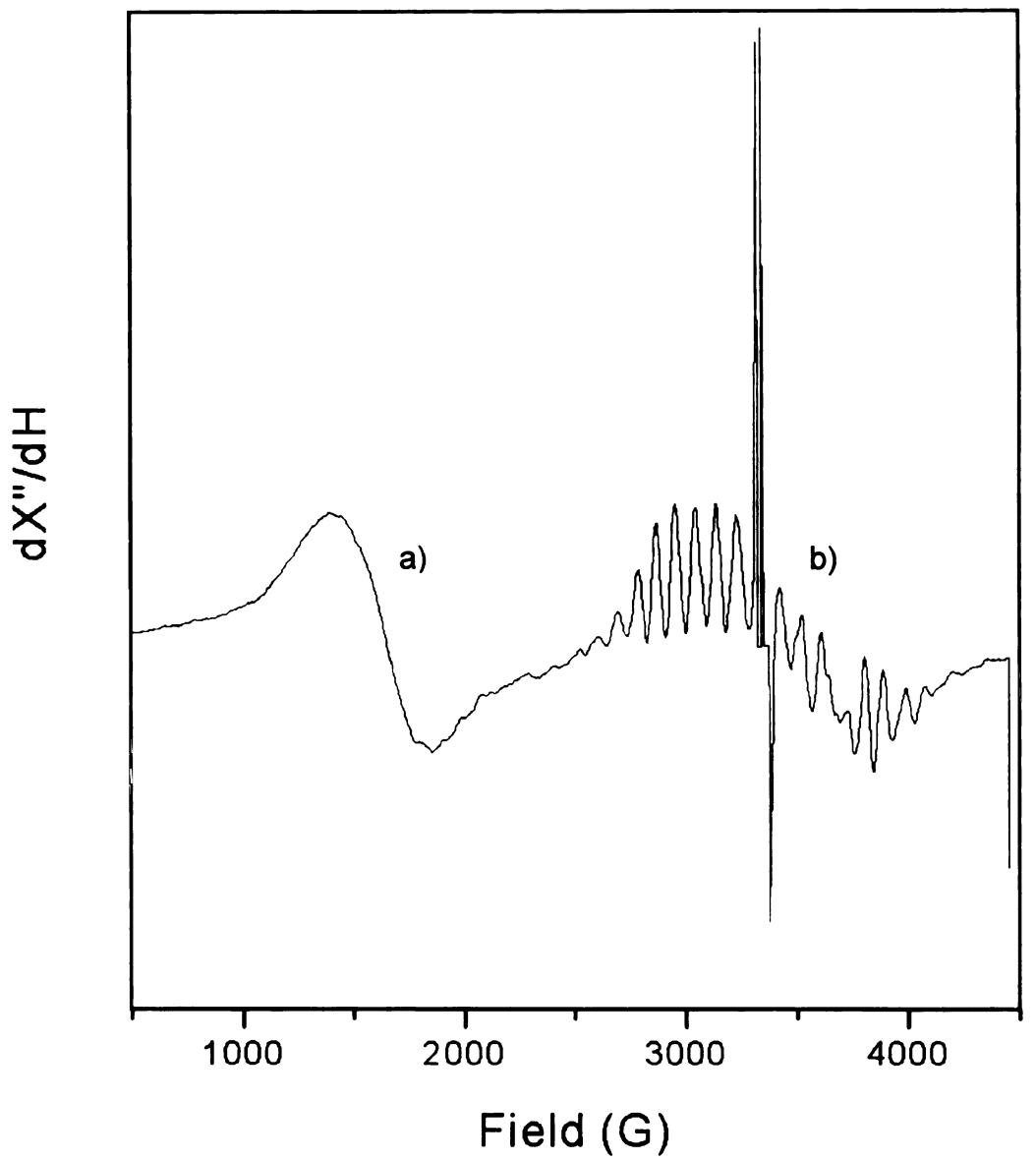

Figure 1-5 The g = 4.1 (a) and multiline (b) EPR signals observed in PSII membranes. This spectrum was kindly provided by Pierre Dorlet.

was later identified as coming from the $S_2Y_z^{\bullet}$ state (*17, 25, 26*). This signal has more recently been simulated by the Babcock (*27*) Britt (*28*), and Brudvig (*29*) groups in order to determine the distance between $(Mn)_4$ and $Y_z^{\bullet}$. From the results of the simulation studies, it was estimated that $(Mn)_4$ and $Y_z^{\bullet}$ are separated by a center-to-center, point-dipolar distance of 8-9 Å.

The oxidation state of each Mn atom in the cluster has been investigated by using X-ray absorbance near-edge spectroscopy (XANES). This technique has been used to detect oxidation state changes of many transition-metal compounds. The results of the study performed on PSII showed significant shifts in the XANES edge positions on going from S_0 to S_1 and from S_1 to S_2 and have been interpreted as manganese-centered oxidations (*30-32*). Oxidation of the manganese cluster on the S_2 to S_3 transition is more controversial with two groups claiming a significant edge shift (*30, 32*) and one group reporting only a minimal shift in the edge position upon this transition (*31*). From XANES studies on model compounds and PSII, the oxidation states of the four manganese atoms are suggested to be: S_0, II, III, IV, IV; S_1, III, III, IV, IV; S_2, III, IV, IV, IV; S_3, IV, IV, IV, IV.

1.2.5 Y_D and Y_z

There are two redox active tryosine residues found in PSII, Y_D and Y_z, which are located in position 161 of the D2 and D1 polypeptides, respectively. The oxidized form of Y_D, gives rise to a dark-stable electron paramagnetic resonance (EPR) signal known as Signal II_s (s = slow) due to its slow relaxation kinetics that are on the order of minutes (for reviews see (*33*)). It is a stable

neutral radical and is believed to be well shielded from solvent (*26, 34*). The tyrosine Y_D does not have a known role in the oxidation of water and will not be discussed further here.

A second tyrosine residue, $Y_z^{\bullet}$, also gives rise to an EPR signal at room temperature in intact systems called Signal II_{vf} (vf = very fast) with fast decay kinetics on the order of microseconds (*35, 36*). In contrast to Y_D, Y_z has a very specific role in water oxidation by functioning as an intermediate cofactor between P_{680} and the manganese cluster. In light of experimental evidence and the role of tyrosine radicals in the general class of metalloradical enzymes (Frey, 1990 #215; Sigel, 1994 #216), it was suggested that Y_z functions by using a hydrogen-atom abstraction mechanism (*37, 38*). The details of the mechanism for water oxidation will be discussed below.

1.2.6 A Model for Water Oxidation

A metalloradical mechanism for water oxidation, proposed by the Babcock laboratory (*39, 40*), invokes $Y_z^{\bullet}$ as a hydrogen atom abstractor from manganese-bound water on each S-state transition. In this model, the two terminal manganese atoms are catalytically active and bind the two substrate water molecules in the S_0 state. Another important feature of this model is charge neutrality. No charge is accumulated on the $(Mn)_4$ cluster, thereby avoiding the high energy situation of creating a charged species in regions of low dielectric. Figure 1-6 illustrates the important details of this mechanism for the S_0 state. Following formation of P_{680}^{+}, Y_z is oxidized in the nanosecond time domain

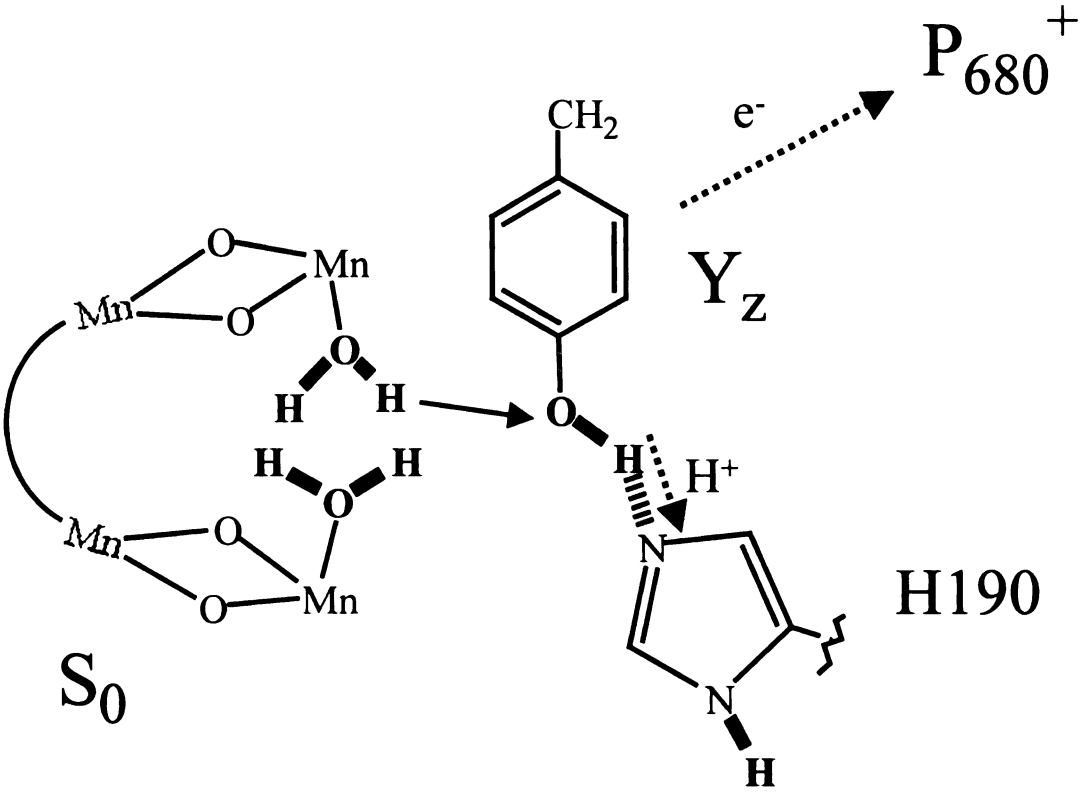

Figure 1-6 Tyrosine Y_z oxidation and reduction in the S_0 state. The dashed arrows illustrate the flow of the electron and proton during Y_z oxidation. The solid arrow shows abstraction of a hydrogen atom by $Y_z^{\bullet}$ during its reduction.

(*41, 42*) and simultaneously deprotonates to a nearby histidine residue (*43-47*), identified by mutagenic and kinetic data as D1-H190 (*48-52*). Subsequently, $Y_z^{\bullet}$ abstracts a hydrogen atom, on the microsecond to millisecond time scale, from a water molecule ligated to the $(Mn)_4$ cluster. This sequence of steps is proposed to occur for each S-state transition as shown in Figure 1-7.

Functions for the Ca^{2+} and Cl^- ions are also proposed in this model (*38*). The Cl^- ion binds to a Ca^{2+} atom that is carboxylate-bridged to the $(Mn)_4$ cluster. After the formation of $S_1Y_z^{\bullet}$, Cl^- migrates to the upper catalytic Mn atom, bringing with it a proton from the lower position. This ensures that an abstractable hydrogen atom is available near $Y_z^{\bullet}$ in the higher S-states. Upon hydrogen atom abstraction in the $S_2 \rightarrow S_3$ transition, the oxo/hydroxyl species is formed. On the $S_3 \rightarrow S_4$ transition, $Y_z^{\bullet}$ abstracts the final hydrogen atom in concert with the formation of an oxygen-oxygen bond and the reduction by one electron of the $(Mn)_4$ cluster. (*37*). Molecular oxygen is released as product and then Cl^- migrates back to the Ca^{2+} site and two water molecules bind to the $(Mn)_4$ cluster to regenerate the S_0 state. This model maintains overall cluster electroneutrality and minimizes nuclear motion, which are both important in terms of the low driving force available to oxidize water and the high turnover numbers (up to 200 electrons per second) that the OEC attains.

1.2.7 The Reduction Rates of $Y_z^{\bullet}$

Upon each S-state transition, $Y_z^{\bullet}$ is formed and is subsequently reduced by the Mn cluster. Central to understanding the S-state mechanism is the kinetics of $Y_z^{\bullet}$ reduction. The rate of $Y_z^{\bullet}$ reduction for each S-state transition was

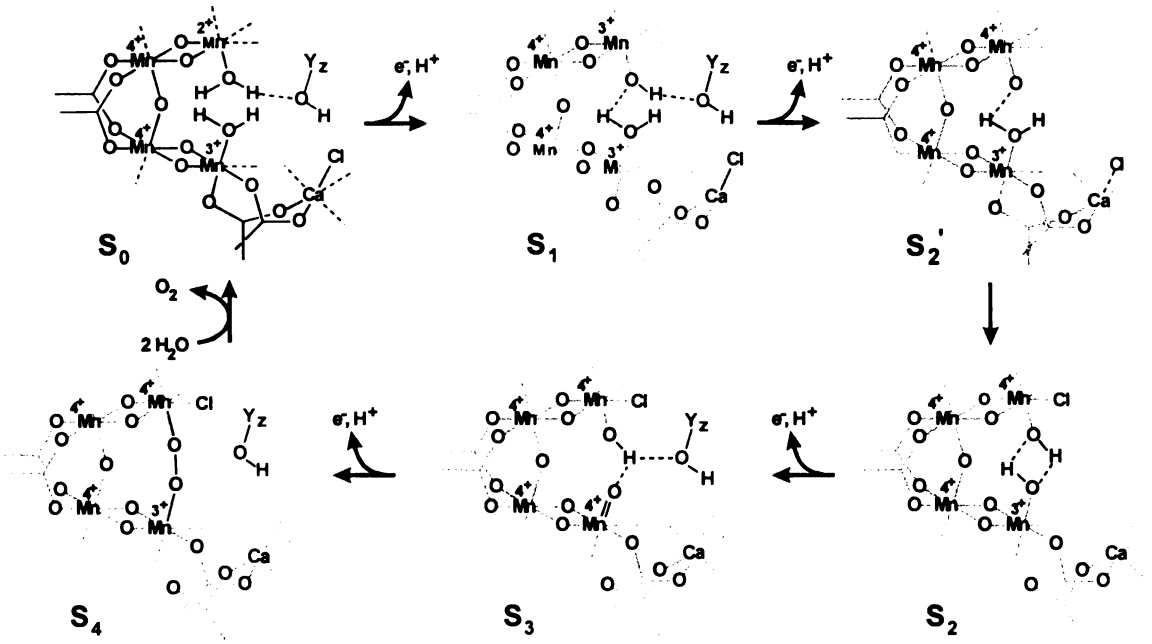

Figure 1-7 A model for the S-state cycle in PSII. This figure was kindly provided by Gerald T. Babcock.

first measured by Babcock in 1976 by using time-resolved electron paramagnetic resonance spectroscopy (EPR) (*53*) and more recently by Razeghifard (*54*). These rates have also been measured by optical absorption spectroscopic techniques in the UV region (Dekker, 1984 #212; Renger, 1986 #213; Rappaport, 1994 #191). The optical approach provides better signal to noise, but requires the use of spectral deconvolution techniques to avoid kinetic interferences from the acceptor side of PSII. Time-resolved EPR, on the other hand, is more convenient since it does not require spectral deconvolution, but is more time consuming because it requires extensive signal averaging to attain adequate signal to noise. In both cases, the decay rates of $Y_z^{\bullet}$ were shown to occur on the μs to ms time-scale depending upon the oxidation state of the $(Mn)_4$ cluster.

The rate of $Y_z^{\bullet}$ reduction by the $(Mn)_4$ cluster has also been studied in PSII samples where the OEC has been chemically, biochemically, or genetically modified. The results of these studies are reported in Table 1 and show a retarding effect on some or all of the S-state transitions. For example, the depletion/repletion of Ca^{2+} [*55, 56*] or the removal of the 33 kDa protein (*57*) has been shown to slow the $S_3 \rightarrow (S_4) \rightarrow S_0$ transition. In addition, Razeghifard et al. showed that $Y_z^{\bullet}$ reduction was slowed to approximately 6 ms on the $S_3 \rightarrow (S_4) \rightarrow S_0$ transition in an engineered strain of cyanobacteria lacking the Mn-stabilizing protein (*58*). All of the above conditions led to a slowdown of the O_2 releasing step in the S-state cycle.

Table 1-1 Half-times for S-state Advance in Various Enzyme Preparation Types - Taken from *(58-61)*

Sample Type	$Y_z^{\bullet}S_1 \rightarrow Y_zS_2$	$Y_z^{\bullet}S_2 \rightarrow Y_zS_3$	$Y_z^{\bullet}S_3 \rightarrow Y_zS_0$
Thylakoids	65-86 μs	140-245 μs	750 μs;1.3 ms
PSII membranes	30-70 μs	55-110 μs	1.2-1.4 ms
PSII core particles	75-95 μs	225-380 μs	4.1-4.6 ms
D61N	240 μs	520 μs	n.d.
-MSP	n.d.	n.d.	6.0 ms
Cl^-	n.d.	n.d.	3.3 ms
Br^-	n.d.	n.d.	4.9 ms
NO_3^-	n.d.	n.d.	15.6 ms
NO_2^-	n.d.	n.d.	8.2 ms
I^-	n.d.	n.d.	11.7 ms

Evidence for perturbations affecting the earlier S-state transitions was also found. For example, the rates of all the S-state transitions are dependent upon the degree to which the system is perturbed in the preparation of PSII membranes. Razeghifard et al. has shown that the treatment of thylakoids to prepare PSII membranes leads to retardation of all S-state transitions, with the largest effect seen on the last transition (*54, 58*). The mutation work done by Hundelt et al. on D1-Asp61 also demonstrated slower $Y_z^{\bullet}$ reduction rates (*61*). When this aspartate residue was mutated to the uncharged species, asparagine, oxygen evolution was retained, but the S-state transitions were retarded. The oxygen-evolving step was slowed by a factor of 9-10. So not only is the $S_3 \rightarrow (S_4) \rightarrow S_0$ transition affected by sample perturbations, but the earlier S-state transitions can be affected as well.

1.2.8 Calcium

In the early 1980s it was shown that Ca^{2+} is needed for efficient oxygen-evolution (*62*). When the 17 and 23 kDa polypeptides were removed from PSII by using a high salt treatment, a substantial amount of oxygen-evolution activity was lost. Successful reactivation of oxygen-evolution activity did not occur upon reconstitution of these polypeptides, but also required long incubation in the presence of excess Ca^{2+}. These experiments ultimately led to the conclusion that the 17 and 23 kDa polypeptides were needed in order to retain Ca^{2+} in its native binding site, and without these polypeptides, excess concentrations of Ca^{2+} were needed in order to support high rates of oxygen-evolution. Without

Ca^{2+} the system is unable to advance past the $S_2Y_z^{\bullet}$ state, and more than 90-95% of oxygen-evolution activity is suppressed.

A study involving the examination of the ability of other metal atoms to replace Ca^{2+} and concurrently support efficient oxygen-evolution has shown that only Sr^{2+} can effectively perform this duty, reactivating about 40% of the original activity (*62*). Substitution of Sr^{2+} for Ca^{2+} results in a modified multiline EPR signal that has narrower hyperfine line splittings (*63, 64*). This result led to the proposal that the Ca^{2+} binding site is close to the Mn cluster and the substitution of Sr^{2+} for Ca^{2+} caused perturbations near the Mn cluster due to its larger ionic radius (1.13 Å, compared to 1.0 Å for Ca^{2+}). Additional evidence to support this proposal has come from EXAFS studies (*65*) and FTIR results showing a Ca^{2+} that is carboxylate-bridged to Mn (*66*). Although it is generally agreed upon that Ca^{2+} is required for efficient oxygen evolution, it is still not known exactly how Ca^{2+} participates in the water oxidation chemistry. Some possible roles for Ca^{2+} have been proposed and are discussed in the following section.

1.2.9 Proposed Roles for Ca^{2+} in Water Oxidation

Although a general consensus for the function of Ca^{2+} has not been reached, several recently proposed models assign a possible role for Ca^{2+}. In general, these roles for Ca^{2+} fall into two categories. In one case, direct involvement of Ca^{2+} in the formation of the oxygen molecule has been suggested (*67-69*). For the second, a more general role for Ca^{2+} involves assisting in the catalytic efficiency of the OEC (*37, 38*). These proposed roles will be discussed along with an experiment devised to test these roles in the function of PSII.

In the first case, the removal of Ca^{2+} would be expected to deter the formation of the O-O bond on the $S_3 \rightarrow (S_4) \rightarrow S_0$ transition. Pecoraro et al. and Limburg et al. postulated that Ca^{2+} presents a hydroxide nucleophile close enough to a putative $Mn^{V}=O$ species to form the critical O-O bond in the S_4 state (*67, 70*). Siegbahn and Crabtree have also employed Ca^{2+} in the O-O bond forming step to provide a solution to the energetic difficulty of forming the reactive oxyl radical (*68*). The proposed five-coordinate, Mn-oxo complex formed in S_3 is unreactive and incapable of forming an O-O bond until it chelates with the calcium complex to become six-coordinate. This allows the reactive Mn^{IV}-$O^{\bullet}$ complex to form, which subsequently leads to O-O bond formation. In these models, O-O bond formation cannot occur without Ca^{2+} in the site, but the cycle of events prior to this step is not expected to be influenced significantly by the depletion of this cofactor. This is especially so if some or all S-state transitions correspond to pure electron tunneling (*71*), as there appears to be consensus that little structural alteration accompanies Ca^{2+} replacement by Sr^{2+} in the OEC (*13, 65, 72*). Likewise, there is no indication of a dramatic change in the driving force for S-state advance when cofactor substitution is carried out. If Sr^{2+} substitution did alter potentials significantly, oxygen evolution would not be possible since the potential span between P_{680}^{+}/P_{680} and water is only about 0.2 V.

For the second class of models, proton-coupled electron transfer provides the mechanistic basis for each S-state advance (*37, 38*). Here, small structural changes will have significant effects on kinetics owing to the much greater

sensitivity of the proton potential surface to distance (*7, 73*). Thus, although Ca^{2+} is necessary for only the higher S-state transitions (*38*), slight perturbations to its geometry or replacement by Sr^{2+} may affect all S-state transitions. This model places Ca^{2+} in close proximity to the Mn cluster but does not directly invoke it for O-O bond formation (*38*). Calcium's function, here, is to act as a docking site for Cl^-, so that Cl^- diffusion into the site does not become rate limiting when it is utilized for charge migration on the S_1 to S_2 transition, (*38*). The oxygen-oxygen bond is formed, in this model, by the concerted reaction between $Y_z^{\bullet}$, Mn^{IV}=O, and Mn^{IV}-OH (*37*). Siegbahn's concerns about the energetics of Mn^{IV}-$O^{\bullet}$ formation disappear in the Hoganson et al. model, as an "energetic boost" is provided by the concerted O-O bond formation event. Calcium is important for efficient O_2 production, but does not play a central role in product formation.

Strontium replacement for Ca^{2+} provides an excellent probe to address these issues. For the first class of models, we would expect the substitution of Sr^{2+} for Ca^{2+} to hinder the O-O bond forming step, thereby causing a pronounced effect on the reduction kinetics of $Y_z^{\bullet}$ on the $S_3 \rightarrow (S_4) \rightarrow S_0$ transition. While for the second class of models, a retardation of all S-state transitions is expected because, in this model, Ca^{2+} plays more of a general role in water oxidation.

1.3 Project Goals

The goal of my thesis research was to investigate the mechanistic predictions of the above models in regards to the role of Ca^{2+} in efficient O_2-evolution, and to subsequently gain more information on the hydrogen atom abstraction mechanism.

To investigate the role of Ca^{2+}, the reduction rate of $Y_z^{\bullet}$ was monitored by using time-resolved EPR spectroscopy for each S-state transition, $S_1 \rightarrow S_2$, $S_2 \rightarrow S_3$, and $S_3 \rightarrow (S_4) \rightarrow S_0$, to determine if each transition was affected by Sr^{2+} substitution or if only the oxygen evolving step was retarded. If the role of Ca^{2+} is to assist in the formation of the O-O bond that ultimately leads to the release of molecular oxygen, then its depletion will hinder the formation of this bond. We expect, then, that only the rate of the $S_3 \rightarrow (S_4) \rightarrow S_0$ transition would be significantly altered, particularly if some, or all, of the earlier S-state transitions involve pure electron transfer. On the other hand, if Ca^{2+} does not play a direct role in bond formation but rather is integral to the active site and plays another catalytic role by, for example, binding Cl^-, then its replacement by Sr^{2+}, which affects the integrity of the OEC only slightly, is likely to affect all S-state transitions.

The second part of my research was to use the results obtained for the reduction of $Y_z^{\bullet}$ in Sr^{2+}-substituted PSII membranes to investigate the hydrogen atom abstraction mechanism proposed for water oxidation. If reduction of $Y_z^{\bullet}$ takes place by a pure electron transfer process, any slight perturbations to the OEC caused by the substitution of Sr^{2+} would have very minute effects, if any, on the rate of the electron transfer process. But, if instead, both a proton and an electron are transferred as a hydrogen atom during $Y_z^{\bullet}$ reduction, then we would expect to see much larger rate alterations, due to the greater dependence of this type of process on donor and acceptor distance and orientation. Thus, the

results of the time-resolved EPR experiments obtained for the Sr^{2+}-substituted PSII samples can lend some insight into the mechanism of $Y_z^{\bullet}$ reduction.

Chapter 2

2 Electron Paramagnetic Resonance Spectroscopy

2.1 Basic Principles

Electron paramagnetic resonance (EPR) is based upon the interaction of radiation of microwave frequency with magnetic moments arising from unpaired electrons. Therefore, the application of EPR spectroscopy is limited to paramagnetic systems. Information regarding the properties of the paramagnetic system is gained by measuring the attenuation versus frequency of a beam of electromagnetic radiation as it passes through the sample. The lines in the spectrum represent transitions between energy levels of the radical species, and their frequency values are a measure of the energy separation of the two levels. The identity of the radical as well as the nature of its surroundings can be gained from an analysis of the pattern and shape of the lines obtained.

Electromagnetic radiation is made up of coupled electric ($\mathbf{E}_1$) and magnetic ($\mathbf{B}_1$) fields perpendicular to the direction of propagation, oscillating at some frequency value. Electromagetic radiation can also be represented as a stream of particles called photons, which have an energy value equal to $h\nu$. Different energy states arise from the interaction of the unpaired electron spin moment ($m_s = \pm \frac{1}{2}$) with the magnetic field component, $\mathbf{B}_1$. This phenomenon, called the Zeeman effect, lifts the degeneracy of the energy levels for the m_s = $+\frac{1}{2}$ and $-\frac{1}{2}$, or as commonly called the α and β states, respectively. The splitting of the energy levels can be varied by changing the static magnetic field, **B**; absorption occurs when the energy ($h\nu$) of the microwave radiation incident on

the

Fig

the

eq

wh

me

mo

spe

ther

exp

loca

at t

spin

0. ½

the sample, equals the splitting of the α and β energy levels of the molecule (see Figure 2-1). This energy value is then used to calculate the Zeeman *g* factor of the radical species giving rise to the observed transition according to the equation:

$$h\nu = g\beta_e \mathbf{B} \qquad (1)$$

where

h = Plank constant

ν = resonant frequency

β_e = Bohr magneton

B = static magnetic field

The g_e factor for a free-electron is equal to 2.0023. Deviation of the measured *g* factor from this free-electron value arises from orbital angular momentum effects and can be used to aid in the identification of the radical species giving rise to the signal.

In addition to the interaction of an electron with an external magnetic field, there is another interaction called nuclear hyperfine coupling. The electron experiences a second field generated by magnetic nuclei in its vicinity. These local fields $\mathbf{B}_{local}$ add vectorially to the external field to produce the total field $\mathbf{B}_{eff}$ at the electron being probed. The neighboring nuclei may possess an intrinsic spin angular momentum with possible nuclear spin quantum number I values of 0, ½, 1, 3/2, 2, ..., etc., with corresponding nuclear spin states given by $2I + 1$.

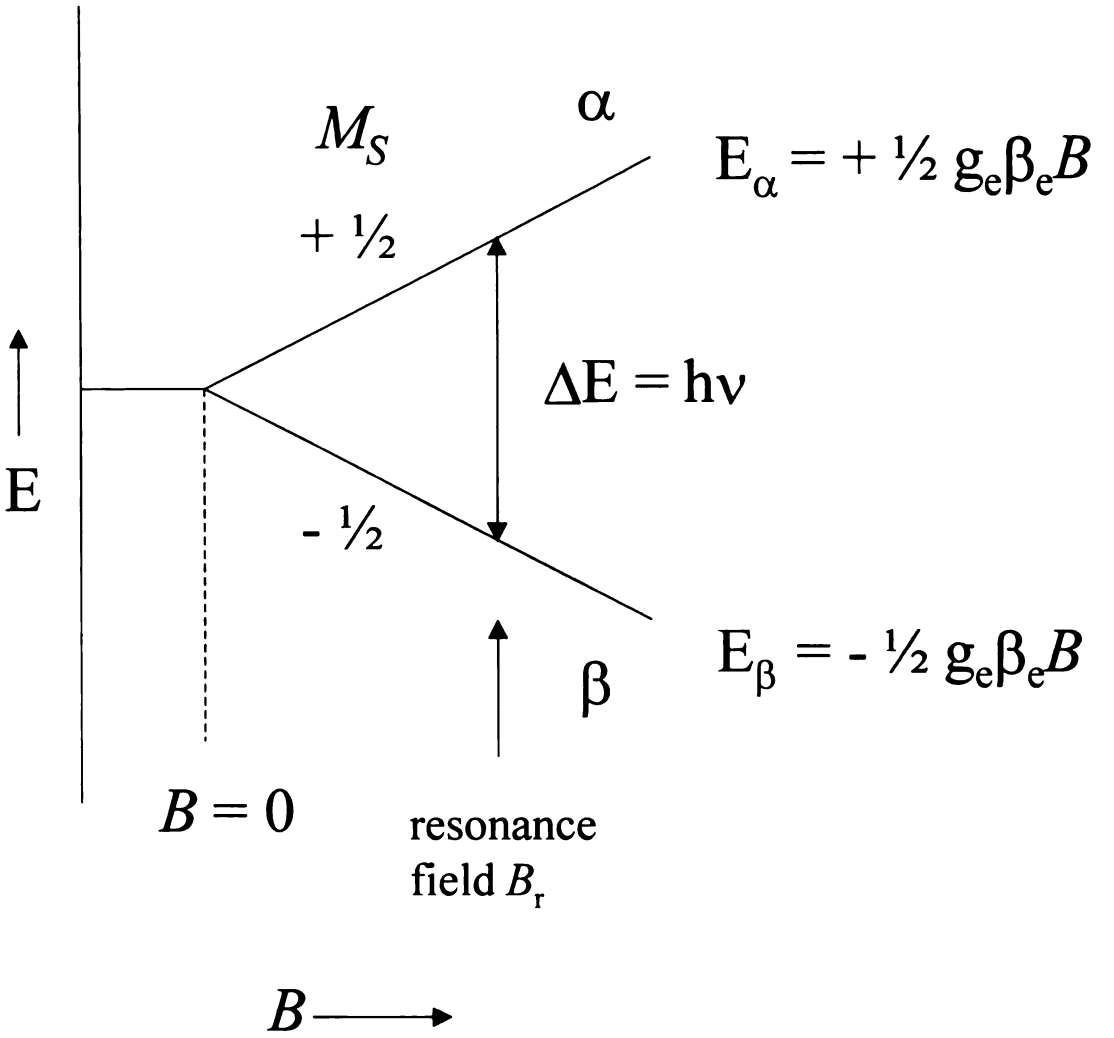

Figure 2-1 Energy level scheme for a free electron as a function of applied magnetic field *B*. Absorption occurs when the incident radiant energy equals the energy-level separation.

The result of electron interaction with neighboring nuclear-dipole moments is a splitting of the resonance, referred to as hyperfine splitting. The nuclear hyperfine interaction splits each of the electron Zeeman energy levels into $2I + 1$ sublevels. Hyperfine interactions assist in the study of paramagnetic species by offering more detailed information in addition to g-factor information gained from interaction of the electron with the external magnetic field.

2.2 The EPR Spectrometer

A block diagram of a typical EPR spectrometer is shown in Figure 2-2. The source of microwave radiation is usually a klystron and the frequency typically used in most EPR spectrometers is approximately 9.5 GHz. The klystron is a vacuum tube that can produce microwave oscillations centered on small frequency ranges. The frequency of the radiation is determined by mechanical tuning of the klystron cavity and by the voltage applied to the klystron. Microwaves are transmitted from the klystron to the cavity through waveguides of a particular size. The most common is the "X band" which uses 12.7 x 25.4 mm OD rectangular brass pipe for the frequency range of 8.2-10.9 GHz. The frequency of the source is tuned to the appropriate resonant frequency of the cavity, which is determined by the dimensions of the cavity. In order to obtain the highest EPR signal sensitivity, the cavity should hold the sample at a maximum of $\mathbf{B}_1$ (the magnetic component of the microwave radiation) and at a minimum of $\mathbf{E}_1$ (the electric component of the of the microwave radiation), and have $\mathbf{B}_1$ perpendicular to the static magnetic field **B**. The source of the static magnetic field **B** is an electromagnet and the magnitude of **B** is measured and

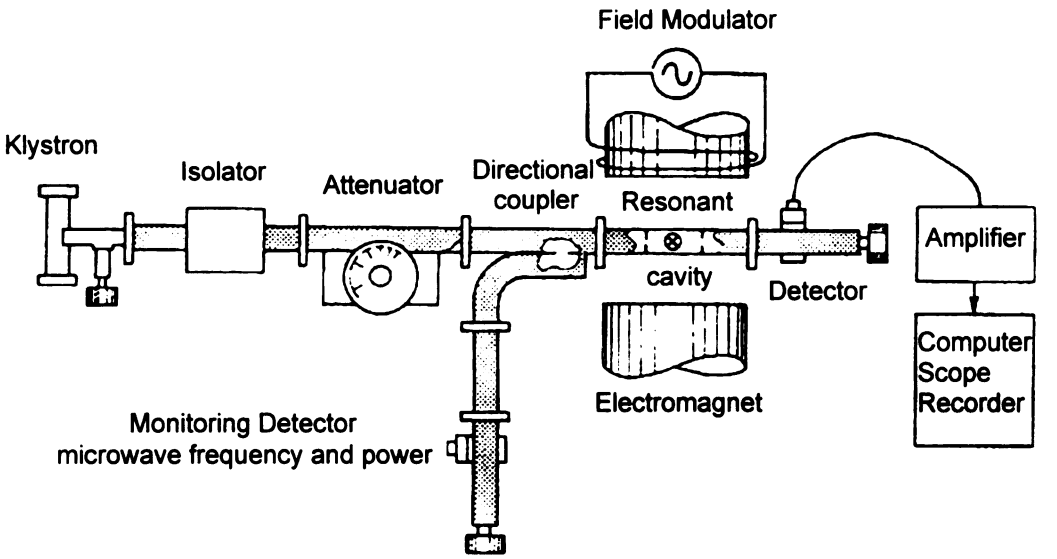

Figure 2-2 Block diagram for a continuous wave EPR spectrometer. Adapted from Electron Paramagnetic Resonance, J.A. Weil, J.R. Bolton, and J.E. Wertz, 1994, John Wiley & Sons. Reprinted by permission of John Wiley & Sons, Inc.

controlled by a Hall-effect detector. Stability in the static magnetic field B is important in order to get accurate measures of the energy level separation ΔE.

The microwave radiation that is produced at the klystron travels through the isolator, which prevents any microwave energy from reflecting back to the klystron, to the attenuator where the microwave power incident on the sample is adjusted. The circulator directs the microwave power to the cavity and simultaneously directs the power reflected from the cavity to the detector. Most often, the frequency of the microwave power is held constant while the magnetic field **B** is varied until the resonant condition is met. At resonance, energy is absorbed by the sample and a change in the power level reflected from the cavity is produced at the detector. Electron paramagnetic resonance spectroscopy employs a technique to increase the signal-to-noise ratio called phase sensitive detection where the magnetic field **B** is modulated at 100 kHz. By modulating **B** the noise-contributing components of frequencies close to or below the modulation frequency are limited. The amplitude of the detected signal will be proportional to the slope of the absorption peak. The output signal appears as the first derivative of the absorption signal where the inflection points of the absorption curve have maximum amplitudes in the first derivative signal and at the resonant field the amplitude is zero.

For time-resolved EPR experiments, the magnetic field B is set to a resonant field value of the species under study, in this case $Y_z^{\bullet}$. For these experiments, the field value chosen is the low-field peak, as indicated in Figure 2-3 by the arrow, and the amplitude of the signal is monitored over time. This field

Figu

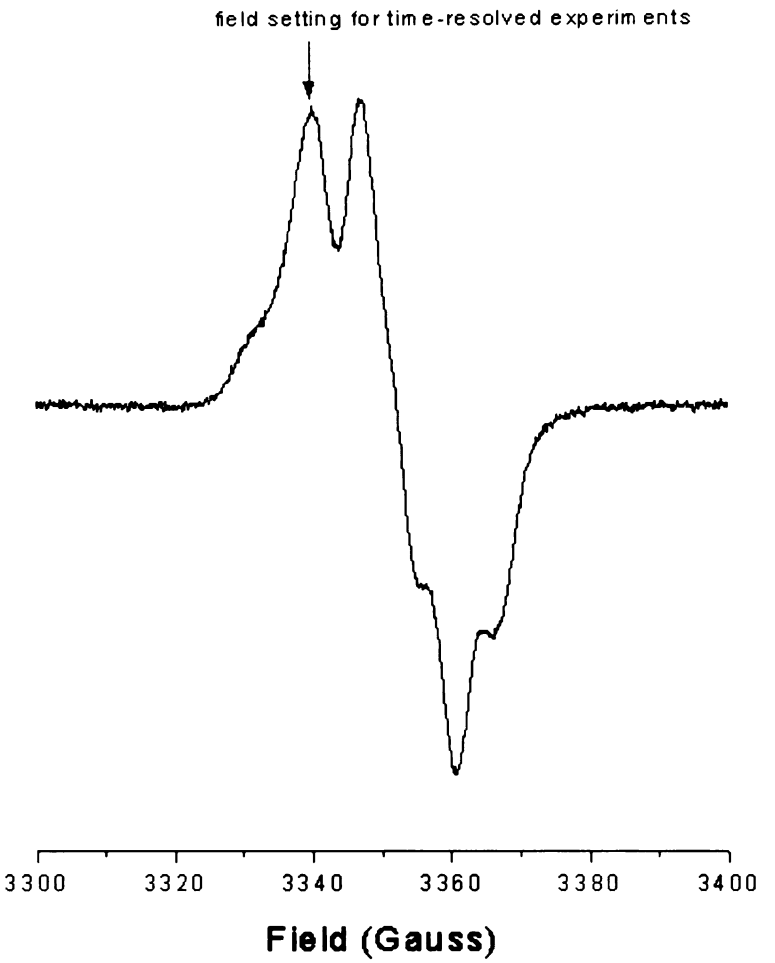

Figure 2-3 Continuous-wave EPR spectrum of $Y_D^{\bullet}$.

value minimizes interference from chlorophyll absorption (Babcock, #222). The principal g-values of the tyrosine radical in PSII have been measured by using high-field EPR spectroscopy and have been reported as g_x=2.0074, g_y=2.0045, and g_z=2.0021. The maximum difference between g_x and g_z corresponds to about nine Gauss at X-Band. The overall bandwidth of $Y_z^{\bullet}$ is much greater than this as the result of hyperfine coupling (Babcock, 1997 #223). Thus, we are confident that setting the field at the low-field peak provides a homogenous sampling of all g-values. Using this technique, the formation and decay of $Y_z^{\bullet}$ can be monitored as the S-states are cycled and its lifetime can be determined.

Chapter 3

3 Materials and Methods

3.1 Preparation of PSII Membranes

Oxygen-evolving PSII membranes can be isolated by detergent solubilization of the chloroplast thylakoid membranes (*74*). These particles, called BBYs, consist of the PSII core with the Mn cluster, Ca^{2+}, Cl^-, the extrinsic polypeptides, and the light harvesting complex, and are nearly devoid of PSI. Further refinement to make core particles with oxygen evolving capacity is possible, where most of the light harvesting complex is stripped away from the OEC (*75*). Both of these preparations have made possible significant advances in the study of the OEC due to the high rates of oxygen evolution activity that can be achieved.

Photosystem II membranes were prepared from fresh market spinach according to the method of Berthold et al. (*74*) with the modifications described in (*76*). The final product is capable of high rates of oxygen evolution and contains very little contamination from PSI. The procedure used in these experiments is as follows:

- About 750 g of market spinach was deveined and washed. The sample was kept at 4° C throughout the isolation procedure.
- The spinach was homogenized in a blender and filtered through a 6-layer cheesecloth. For every 300 g of spinach, 250 mL of grinding buffer containing 0.4 M NaCl, 2.0 mM $MgCl_2 \cdot 6H_2O$, 1.0 mM EDTA, and 2.0 g/L BSA,

20.0 mM *N*-2-hydroxyethylpiperazine-*N'*-2-ethanesulfonic acid (HEPES), pH 7.5 was used.

- The filtrate was centrifuged in a GSA rotor until 1,000 RPM was reached in order to remove large fragments. The supernate was centrifuged for 12 min. at 10,000 RPM.
- The pellet was resuspended by using a paint brush into the first resuspension buffer containing 0.15 M NaCl, 0.40 mM $MgCl_2 \cdot 6H_2O$, and 20.0 mM 2-(*N*-morpholino)ethanesulfonic acid (MES), pH 6.0 homogenized in a glass-teflon homogenizer, and centrifuged for 12 min. at 10,000 RPM.
- The pellet was resuspended by using a paint brush into the second resuspension buffer containing 15.0 mM NaCl, 0.50 mM $MgCl_2 \cdot 6H_2O$, 1.0 mM ascorbic acid and 50.0 mM MES, pH 6.0 and homogenized.
- The chlorophyll concentration was determined by measuring the absorbance values at 645 nm and 663 nm in 80% acetone and then adjusted to 2 mg/mL. A 25% Triton X-100 solution was added dropwise to the stirring sample in the dark to reach a detergent to Chl ratio of 30:1.
- After a 30-minute incubation period in complete darkness, the sample was centrifuged for 30 minutes at 20,000 RPM.
- The pellet was resuspended by using a paint brush into a buffer called SMN containing 15.0 mM NaCl, 0.40 M sucrose, and 50.0 mM MES, pH 6.0 homogenized, and centrifuged for 30 min. at 20,000 RPM.
- The pellet was resuspended by using a paint brush into SMN buffer to a final chl concentration of about 4 mg/mL.

- The final PSII membrane sample was saved in 1 mL aliquots and stored at – 80° C.

3.2 Calcium Depletion of PSII Membranes

Salt-washed membranes were prepared as in Boussac and Rutherford (*63*) as follows:

- PSII membranes were diluted to a chl concentration of 1 mg/mL and incubated in room light for 30 minutes at 4°C in a SMN buffer containing 0.30 M sucrose, 2.4 M NaCl, and 25 mM MES, pH 6.5 at a 1:1 ratio.
- Following incubation 50 μM EGTA was added. The sample was centrifuged for 20 min. at 20,000 RPM.
- The pellet was resuspended in a SMN buffer containing 0.30 M ultra-pure sucrose (Aristar, BDH Laboratory Supplies, United Kingdom), 30 mM NaCl, 50 μM EGTA, and 25 mM MES, pH 6.5.
- After homogenization, 50 μM EGTA was added and the sample was centrifuged for 20 min. at 20,000 RPM.
- The pellet was resuspended in a SMN buffer containing 0.30 M ultra-pure sucrose, 15 mM NaCl, and 25 mM MES, pH 6.5, to a final chl concentration of 2 mg/mL.

3.3 Sample Preparation for EPR Experiments

Reconstitution of the Ca^{2+}-depleted samples was carried out by adding $CaCl_2$ or $SrCl_2$ to a final concentration of 15 mM. Prior to flash illumination 100 μM PPBQ in DMSO and 1 mM ferricyanide were added to the sample. For the pH studies, the salt-washed PSII membranes were resuspended in the same

buffer, but at a pH of 5.9, 6.5 or 7.1. For the istope exchange studies, salt-washed PSII membranes were exchanged into a MN buffer containing 15 mM NaCl, 25 mM MES (pD 6.5) in 99.9% D_2O with a final addition of 15 mM $SrCl_2$. The preparation of the sample was identical to that above, except that the final washing steps were performed in a D_2O-MN buffer. The rate of isotope exchange has been shown to occur in a matter of minutes or less, well within the time it takes to carry out the final washing steps (*77-80*).

3.4 Time-Resolved EPR Experiment Setup

EPR spectroscopy was performed at room temperature with a Bruker ESP 300E spectrometer equipped with a TM_{011} cavity. The spectrometer was tuned to the low-field peak of the stable Y_D radical (D2-Y160) and the kinetic traces obtained for Y_Z oxidation and its subsequent reduction were recorded at this field value. The experiments under steady state flashing light conditions were carried out by using a 350 μL capacity suprasil quartz flat cell (Wilmad, Buena, NJ). Each sample received 100 flashes before being replaced by a fresh sample. For the S-state resolved studies, a home-built, continuous-flow system that is depicted in Figure 3-1 was used to provide fresh samples to the flat cell mounted in the cavity. Each sample received a train of three flashes before being replaced. A pump (Gilson, Inc., Middleton, WI) was used to control the flow rate so that a fresh, dark-adapted sample was supplied for each flash sequence. Following flash illumination, the sample was recycled to a reservoir that was held at 4 °C and kept in absolute darkness for 15 minutes. Each experiment was completed in approximately five hours with about 2000 scans averaged.

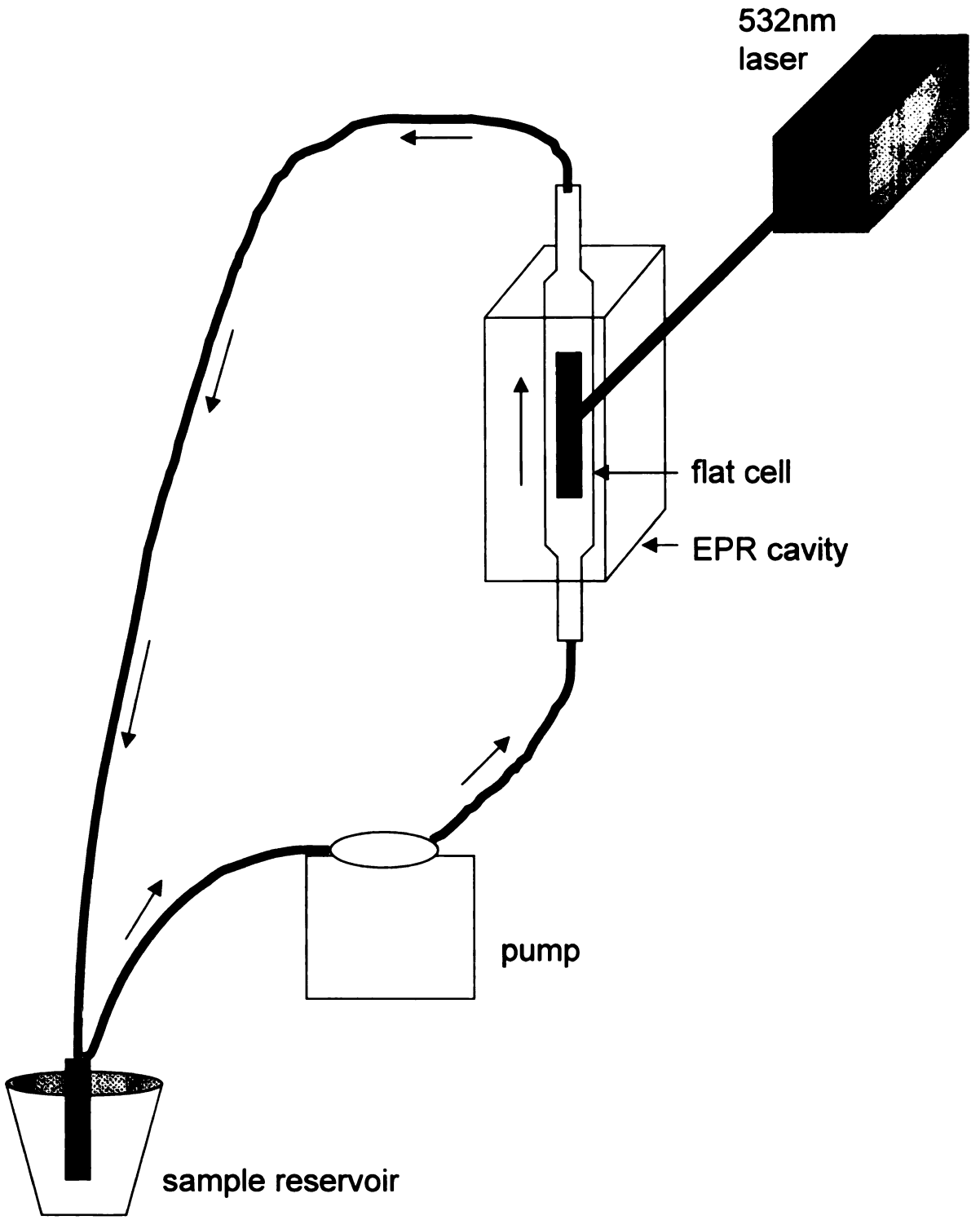

Figure 3-1 Setup for the time-resolved EPR experiments. Flowing the sample allows the formation and decay of Y_z to be monitored for each S-state transition. Sample averaging is possible by recycling the enzyme.

Photoexcitation of the sample at 532 nm was accomplished by using a Quanta-Ray DCR-11 pulsed Nd-YAG laser (Spectra-Physics, Mountain View, CA). A personal computer equipped with a Metrabyte WAAG board and a Metrabyte CTM-05 timing board was used to trigger both the EPR spectrometer and the laser (*81*). The EPR conditions for each experiment are given in the figure legends. A least-squares fitting routine (Origin 5.0, Microcal Software, Inc., Northampton, MA) was used to analyze the kinetic traces.

Oxygen evolution activity was measured with a Clark type electrode under continuous illumination with saturating white light from two projector lamps of 250 W each that are filtered through a $CuSO_4$ solution. Oxygen evolution rates for intact BBYs measured at a concentration of 1 mg/mL chl in SMN buffer, pH 6.0 were typically between 650-750 μmol O_2/mg chl·h while salt-washed, Ca^{2+} and Sr^{2+} reconstituted samples measured at a concentration of 10 μg/mL chl in SMN buffer, pH 6.5 were typically 450-550 and 200-300 μmol O_2/mg Chl·h, respectively. Ferricyanide and DCBQ, at concentrations of 600 μM and 300 μM, respectively, were used as the electron acceptors for these measurements.

Chapter 4

4 Results of Time-Resolved EPR Experiments

4.1 S-State Mixed Kinetics

The formation and decay of $Y_z^{\bullet}$ was monitored under steady state flashing light conditions by setting the magnetic field to the low-field peak of the stable Y_D radical (see Figure 2-3) and inducing the oxidation and reduction of Y_z by using 532 nm laser flashes. Figure 4-1 shows the kinetic EPR traces of the decay of $Y_z^{\bullet}$ in salt-washed PSII membranes reconstituted with either Ca^{2+} (trace a) or Sr^{2+} (trace b). The number of spins was determined by comparing the amplitudes of each kinetic trace to one obtained under the same experimental conditions for a tris-washed sample, which generates one $Y_z^{\bullet}$ spin per reaction center (*82*). Using this procedure, we estimate that 0.5 spin per reaction center for the Ca^{2+}-reconstituted sample was produced on each flash, which is in agreement with values reported by this laboratory (*81*) and reports on intact PSII membranes by other labs (*36, 58*). The Sr^{2+}-reconstituted sample, however, showed a 20% increase in spins due to the slowdown of $Y_z^{\bullet}$ reduction in the $S_0 \rightarrow S_1$ transition, which is sufficiently slowed in the Sr^{2+} sample that its detection is now possible (see below). The lower apparent $Y_z^{\bullet}$ spin count in O_2-evolving samples relative to tris-washed material may be due to broadening of its EPR signal by the $(Mn)_4$ cluster. In Ca^{2+}-depleted samples, $Y_z^{\bullet}$ is in close association with Mn, which broadens its EPR signal at lower temperatures (*25, 27, 83*). Similar effects could

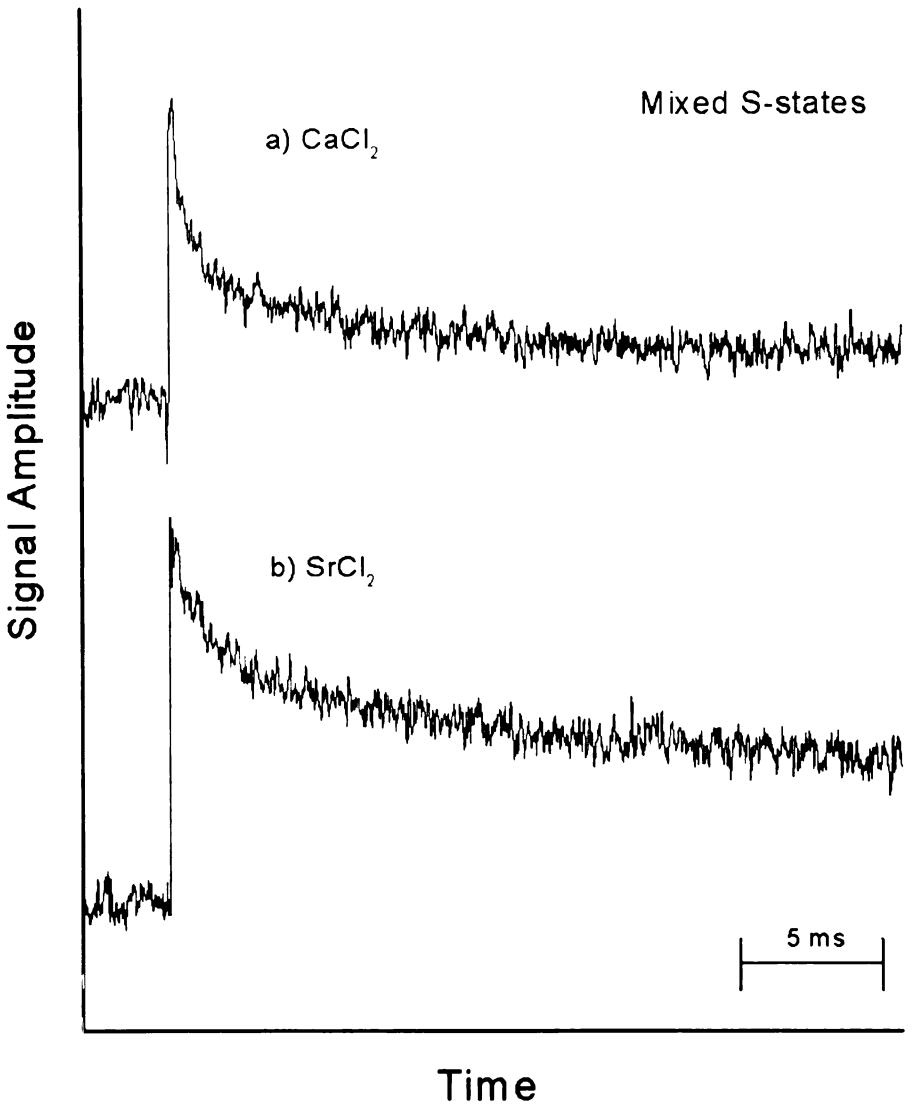

Figure 4-1 Time-resolved EPR steady state kinetic traces (S-states are mixed) for $Y_z^{\bullet}$ reduction in salt-washed PSII membranes reconstituted with (a) $CaCl_2$ or (b) $SrCl_2$. Experimental conditions: Time constant 40 μs, modulation amplitude 4 G, gain 1 x 10^5, microwave power 3 dB, frequency 9.78 GHz, magnetic field locked at low field peak (3470 G), room temperature, flash frequency 0.66 Hz. 2000 events were averaged.

operate in O_2-evolving samples and cause an apparent decrease in spin concentration.

Each kinetic trace in Figure 4-1 shows a biphasic decay. For the Ca^{2+}-reconstituted sample, the fast phase, which is approximately 50% of the total amplitude, is attributed to the reactions $S_1Y_z^{\bullet} \rightarrow S_2Y_z$ and $S_2Y_z^{\bullet} \rightarrow S_3Y_z$, while the slow phase, which is approximately 35% of the total amplitude, is produced from the $S_3Y_z^{\bullet} \rightarrow (S_4) \rightarrow S_0Y_z$ reaction. The remaining 15% of the total amplitude is attributed to the decay of $Y_z^{\bullet}$ in damaged centers that behave like tris-washed PSII membranes. A laser flash artifact is detected on each flash and does not completely cancel with subtraction of an off-resonance trace obtained at 3400 G. This should not greatly interfere with the rate determination of the decaying phases of the kinetic traces. The Ca^{2+}-reconstituted sample (trace a) shows half-times of ~300 μs and ~4 ms for the fast and slow phase, respectively. The Sr^{2+}-reconstituted sample (trace b) has a greater amplitude due to contributions to the fast phase by $S_0 \rightarrow S_1$. The half-times are ~900 μs and ~15ms for the fast and slow phase, respectively. Comparisons of the two kinetic traces shown in Figure 4-1 show that Sr^{2+}-reconstitution apparently slows the rate of $Y_z^{\bullet}$ reduction on all S-state transitions and also shows an increase in the signal amplitude due to the additional detection of $S_0 \rightarrow S_1$.

4.2 S-State Resolved Kinetics

In order to study the effects of Sr^{2+}-reconstitution on the rates of $Y_z^{\bullet}$ reduction in more detail, we resolved the S-state transitions individually as demonstrated in Figure 4-2. To perform this experiment, a sample that was

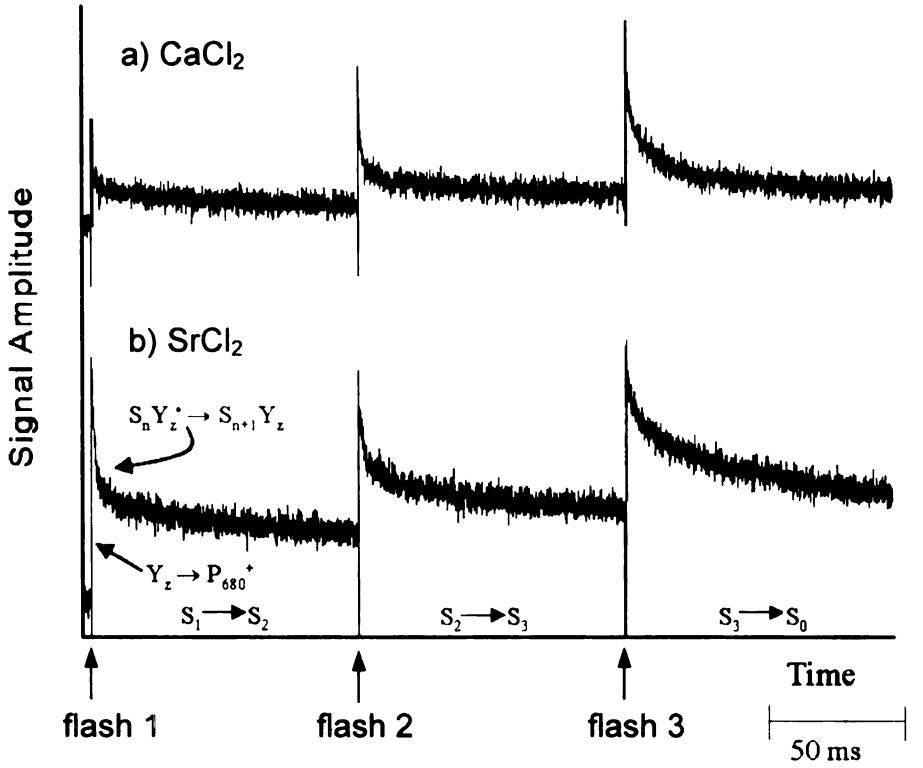

Figure 4-2 Three-flash S-state resolved EPR kinetic traces. Flash one induces the formation of $Y_z^{\bullet}$. Decay of the signal represents the reduction of $Y_z^{\bullet}$ by the $(Mn)_4$ cluster.

poised in the S_1 state by dark adaptation was flowed into the flat cell and given three saturating flashes. The flow rate was adjusted so that each sample received three flashes spaced 100 ms apart before it was replaced by the next dark-adapted aliquot. The first flash initiated the transition $S_1Y_z^{\bullet} \rightarrow S_2Y_z$, while the second flash generated primarily $S_2Y_z^{\bullet} \rightarrow S_3Y_z$. The final flash caused $Y_z^{\bullet}$ reduction on the $S_3Y_z^{\bullet} \rightarrow (S_4) \rightarrow S_0Y_z$ transition, with a small contribution from the other states that is caused by double hits and misses. Figure 4-3 shows kinetic traces and best fits for the first flash given to salt-washed PSII membranes reconstituted with either Ca^{2+} (trace a) or Sr^{2+} (trace b). Both traces show biphasic behavior with the fast phase being attributed to the decay of $Y_z^{\bullet}$ upon the $S_1Y_z^{\bullet} \rightarrow S_2Y_z$ transition and the slow phase to reduction of $Y_z^{\bullet}$ in damaged centers. The reduction of $Y_z^{\bullet}$ on the first flash for the Ca^{2+}-reconstituted sample (trace a) has a half-time of ~200 μs. The Sr^{2+}-reconsitituted sample displayed slower reduction kinetics on the $S_1Y_z^{\bullet} \rightarrow S_2Y_z$ transition (trace b) with a half-time of ~900 μs. The spin counts for each of the above kinetic traces were 0.40 and 0.90 spins for the Ca^{2+}-reconstituted and the Sr^{2+}-reconstituted samples, respectively. The greater number of spins from the Sr^{2+}-reconstituted sample was in part due to the additional detection of the $S_0 \rightarrow S_1$ transition, to Y_z sites in centers deficient in O_2 evolution, and to $Y_D^{\bullet}$ generation on the first flash. The remaining increase is most likely due to S-state dependent effects caused by magnetic interaction between the tyrosyl radical and the manganese cluster that produce small differences in the $Y_z^{\bullet}$ lineshape. These later effects will not

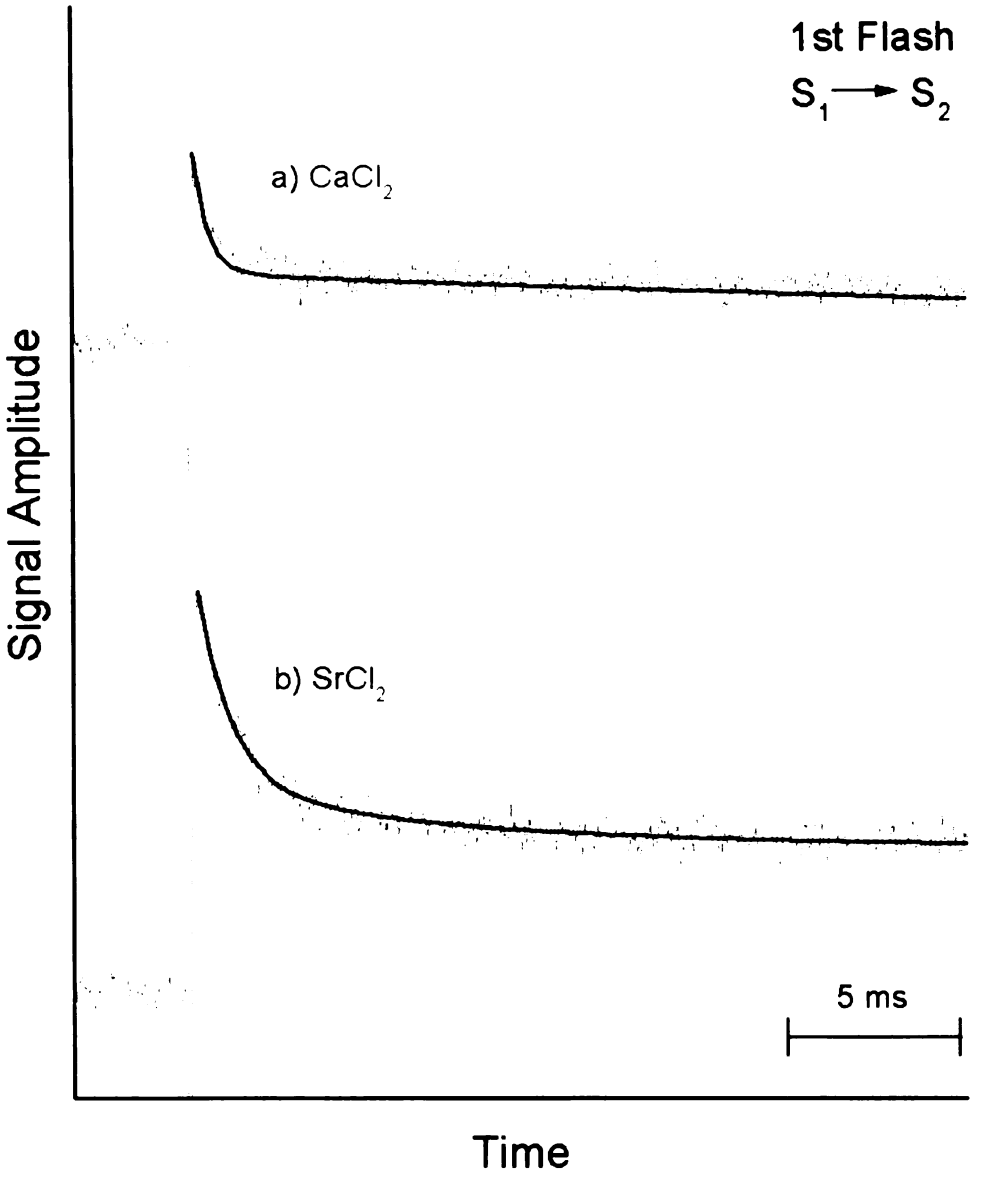

Figure 4-3 Time-resolved EPR kinetic traces for the $S_1Y_z^{\bullet} \rightarrow S_2Y_z$ transition triggered by the first flash in a three flash experiment. Salt-washed PSII membranes reconstituted with (a) $CaCl_2$ or (b) $SrCl_2$ were used. Experimental conditions: Time constant 20 μs in (a) and 40 μs in (b), modulation amplitude 4 G, gain 1 x 10^5, microwave power 3 dB, frequency 9.78 GHz, magnetic field locked at low field peak (3470 G), room temperature. 4000 events were averaged.

substantially alter the fast kinetics that are the primary focus of this study and will not be discussed further.

The kinetic traces for the second transition are shown in Figure 4-4. The S-state advance, $S_2Y_z^{\bullet} \rightarrow S_3Y_z$, showed a slow down in the Sr^{2+}-reconstituted sample that was similar to that of the first flash. The half-times calculated for the Ca^{2+}-reconstituted and Sr^{2+}-reconstituted samples were ~450 μs and ~1.3 ms, respectively. The spin count, 0.50, is nearly the same for both sample types. Figure 4-5 shows the kinetic traces for Ca^{2+}- and Sr^{2+}-reconstituted samples on the $S_3Y_z^{\bullet} \rightarrow (S_4) \rightarrow S_0Y_z$ transition. Due to mixing of the S-state transitions by the third flash, the decays also had a small contribution from the earlier and faster S-state transitions. In addition, the amplitude of these traces increased, compared to the second flash, to a spin count of about 0.55. The half-times were ~5.0 ms and ~18 ms for Ca^{2+}- and Sr^{2+}-reconstituted samples, respectively. The results of the steady-state and S-state resolved experiments are presented in Table 4-1.

4.3 Effects of pH and Isotope Exchange

The effects of pH on the reduction rates of $Y_z^{\bullet}$ in the salt-washed, Sr^{2+}-reconstituted samples were investigated to determine if a pH optimum for $Y_z^{\bullet}$ reduction becomes apparent in any of the S-state transitions upon metal substitution. The effects of pH were studied by carrying out the S-state resolved, three-flash experiment at pH values of 5.9, 6.5, and 7.1 in Sr^{2+}-reconstituted samples. The results of this experiment, shown in Figure 4-6, indicate that there is no substantial effect of pH on the kinetics of $Y_z^{\bullet}$ reduction by the Mn cluster in the 5.9 to 7.1 range. A similar lack of pH effects in the physiological range have

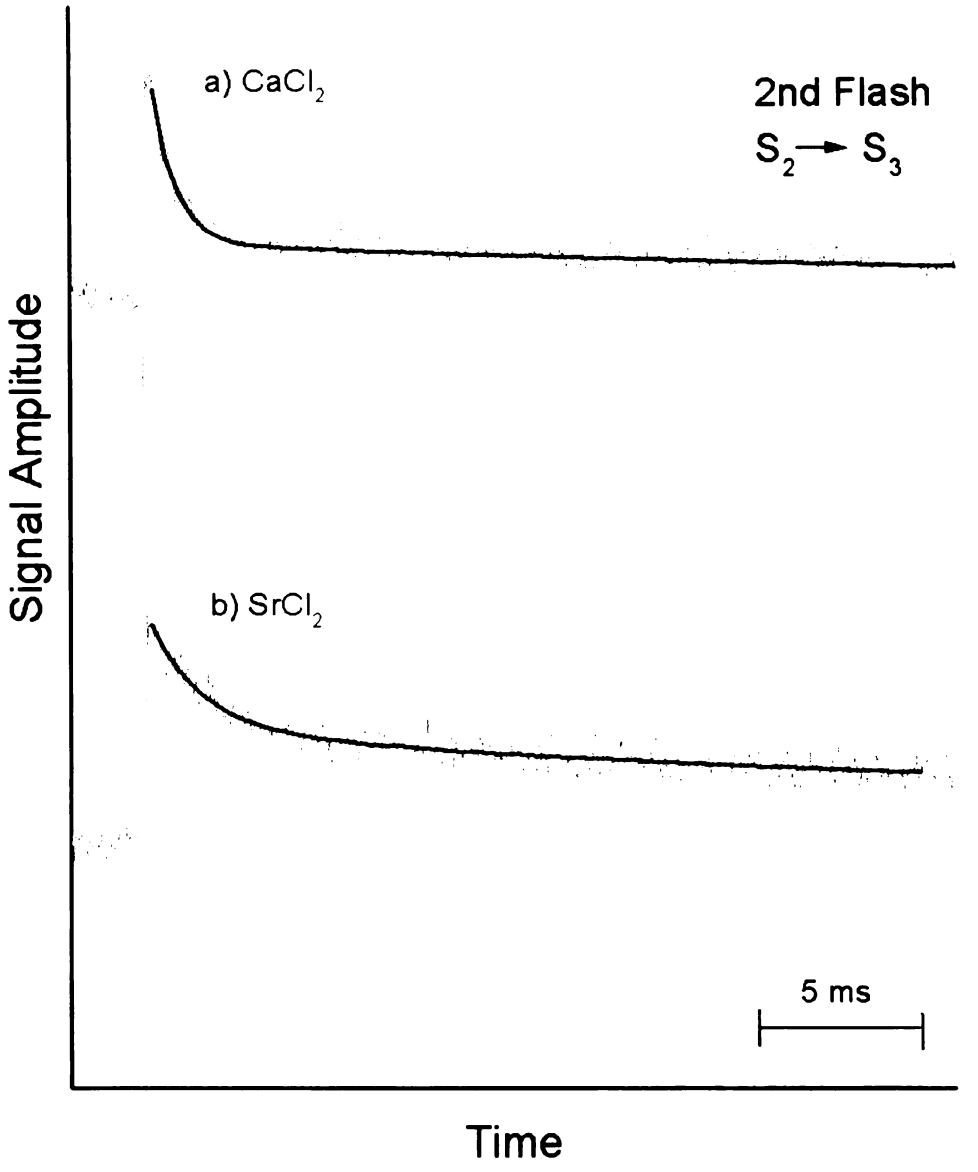

Figure 4-4 Time-resolved EPR kinetic traces for the $S_2Y_z^{\bullet} \rightarrow S_3Y_z$ transition triggered by the second flash in a three flash experiment. Salt-washed PSII membranes reconstituted with (a) $CaCl_2$ or (b) $SrCl_2$ were used. Experimental conditions: Time constant 20 μs in (a) and 40 μs in (b), modulation amplitude 4 G, gain 1 x 10^5, microwave power 3 dB, frequency 9.78 GHz, magnetic field locked at low field peak (3470 G), room temperature. 4000 events were averaged.

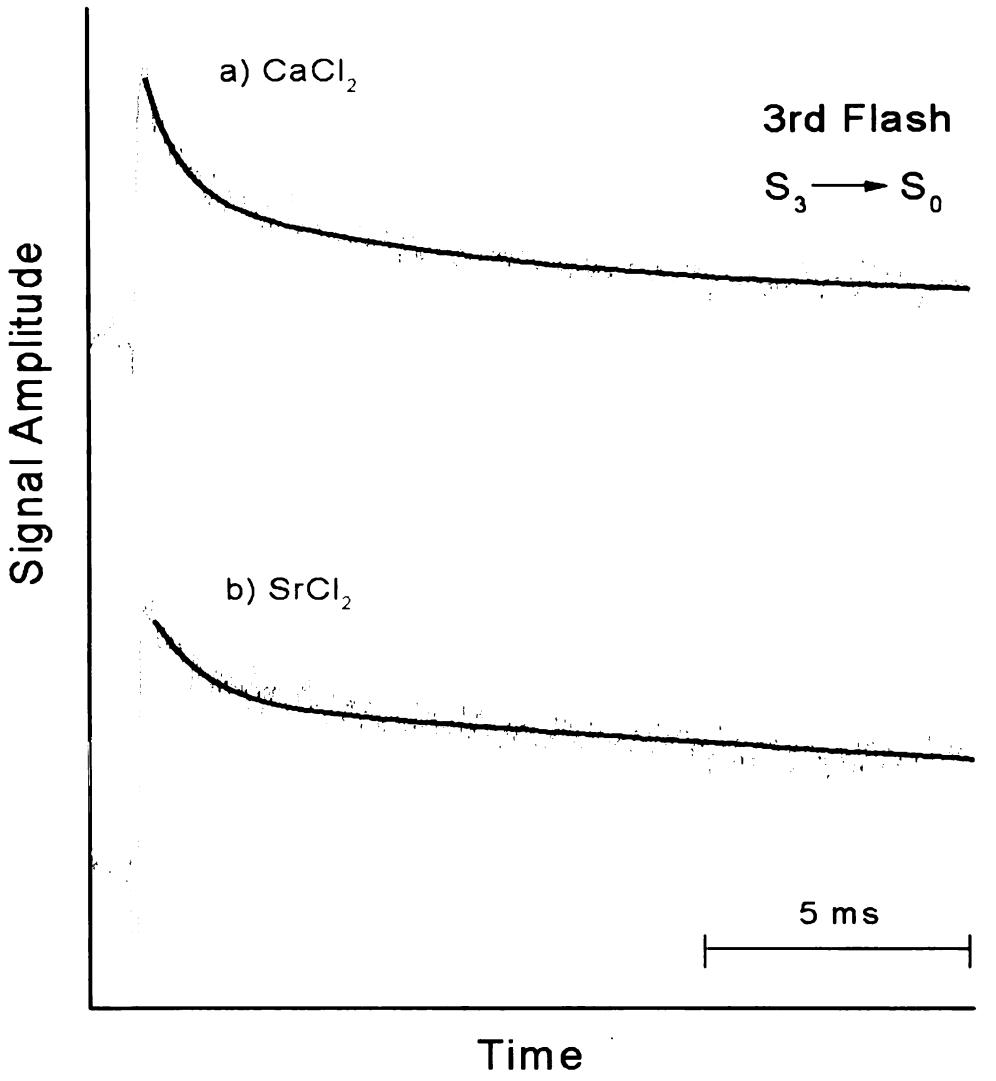

Figure 4-5 Time-resolved EPR kinetic traces for the $S_3Y_z^{\cdot} \rightarrow S_0Y_z$ transition triggered by the third flash in a three flash experiment. Salt-washed PSII membranes reconstituted with (a) $CaCl_2$ or (b) $SrCl_2$ were used. Experimental conditions: Time constant 20 μs in (a) and 40 μs in (b), modulation amplitude 4 G, gain 1 x 10^5, microwave power 3 dB, frequency 9.78 GHz, magnetic field locked at low field peak (3470 G), room temperature. 4000 events were averaged.

Table 4-1 Rates of $Y_z^{\bullet}$ Reduction for Ca^{2+}- or Sr^{2+}-Reconstituted PSII Membranes Determined by Time-Resolved EPR Spectroscopy.

S-state	spin	$^{*}t_{1/2\ (slow)}$	$^{*}t_{1/2\ (fast)}$
Steady-state			
Ca^{2+}	0.50	4 ms (35%)	300 μs (50%)
Sr^{2+}	0.60	15 ms (35%)	900 μs (50%)
$S_1 \rightarrow S_2$			
Ca^{2+}	0.40	40 ms (15%)	200 μs (85%)
Sr^{2+}	0.90	40 ms (15%)	900 μs (85%)
$S_2 \rightarrow S_3$			
Ca^{2+}	0.50	40 ms (15%)	450 μs (85%)
Sr^{2+}	0.50	40 ms (15%)	1.3 ms (85%)
$S_3 \rightarrow S_0$			
Ca^{2+}	0.55	40 ms (15%)	5 ms (85%)
Sr^{2+}	0.55	40 ms (15%)	18 ms (85%)

* The rates here are reported as half-times to be consistent with the Photosystem II literature.

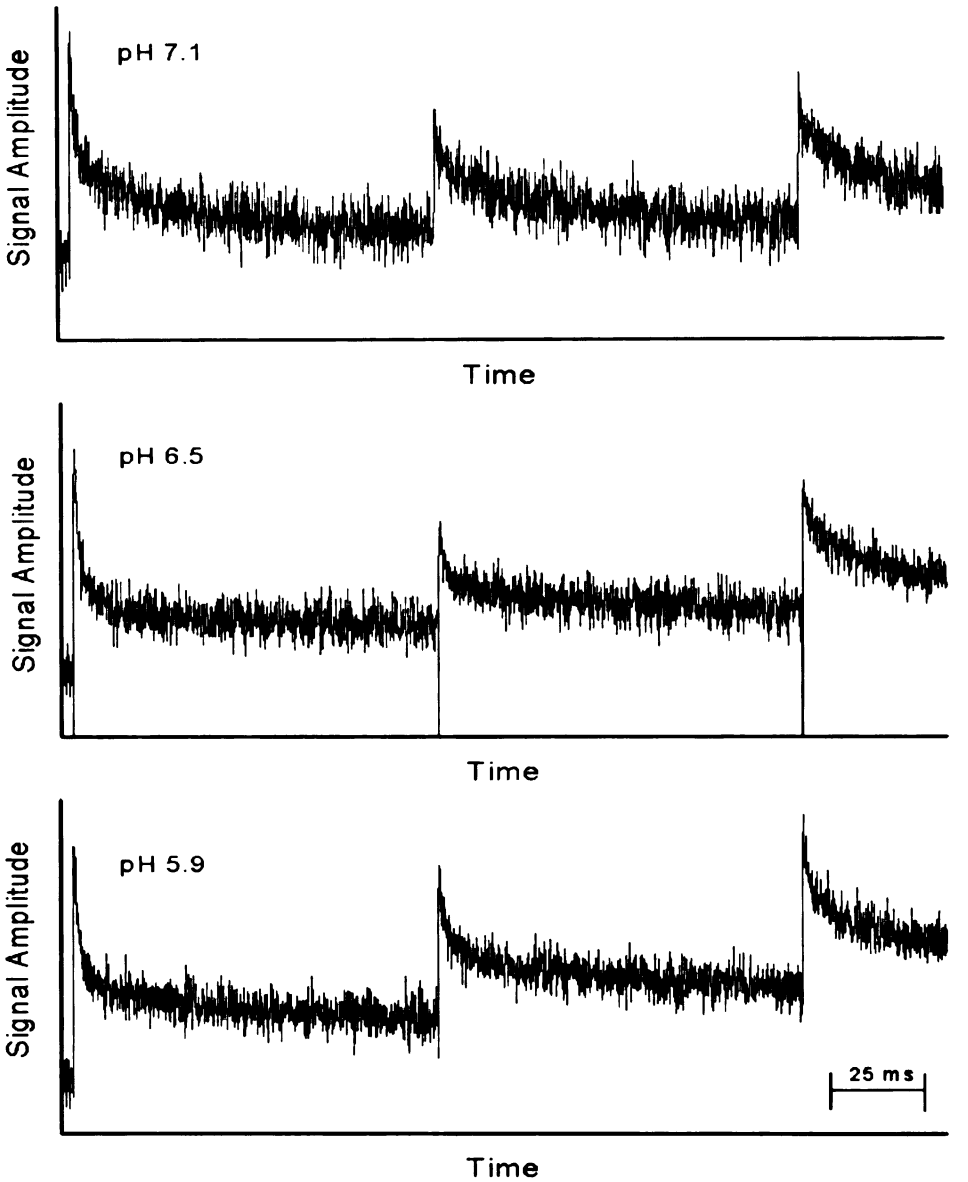

Figure 4-6 Time-resolved EPR kinetic traces for the $S_1Y_z^{\cdot} \rightarrow S_2Y_z$, $S_2Y_z^{\cdot} \rightarrow S_3Y_z$, $S_3Y_z^{\cdot} \rightarrow S_0Y_z$ transitions in salt-washed, Sr^{2+}-reconstituted PSII membranes resuspended in buffers at pH = 5.9, 6.5, 7.1. Experimental conditions: Time constant 40 μs, modulation amplitude 4 G, gain 1 x 10^5, microwave power 3 dB, frequency 9.78 GHz, magnetic field locked at low field peak (3470 G), room temperature. 2000 events were averaged.

been reported earlier for the unperturbed, O_2-evolving system (*84*).

In addition, a hydrogen/deuterium isotope effect study was performed. Deuterium kinetic isotope effects on $Y_z^{\bullet}$ reduction have been carried out in oxygen-evolving PSII membranes by using optical (*60*) and EPR (*85*) methods. These experiments were performed in light of the proposal that $Y_z^{\bullet}$ reduction is accompanied by proton transfer from substrate water. This proposal suggests the possibility of significant kinetic H/D isotope effects, but the results of both the optical and EPR studies showed moderate deuterium kinetic isotope effects on the reduction of $Y_z^{\bullet}$. The k_H/k_D values obtained range from 1.3 to 2.9, depending on the S-state transition, which suggests that the reduction of $Y_z^{\bullet}$ is not severely limited by proton transfer in the intact system.

Deuterium kinetic isotope effect studies on the reduction rate of $Y_z^{\bullet}$ in salt-washed, Sr^{2+}-reconstituted PSII membrane fragments were conducted in this work in efforts to test suggestions that perturbations to the OEC, caused by Sr^{2+}-substitution, hinders proton transfer during $Y_z^{\bullet}$ reduction. The rate of proton transfer is dependent upon donor and acceptor distance to a much greater degree than electron transfer, and therefore is expected to rate limit $Y_z^{\bullet}$ and lead to large deuterium kinetic isotope effects (*86*). In order to test this theory, salt-washed PSII membrane fragments were exchanged into a MN buffer containing 15 mM NaCl, 25 mM MES (pD 6.5) in 99.9% D_2O with a final addition of 15 mM $SrCl_2$. The preparation of the sample was identical to that of the experiments performed above on samples in H_2O, except that the final washing steps were performed in a D_2O-MN buffer. The rate of isotope exchange has been shown to

occur in a matter of minutes or less, well within the time it takes to carry out the final washing steps (*77-80*). Analysis of the flash-induced kinetic traces that are shown in Figure 4-7 for a steady state experiment shows a kinetic isotope effect similar to that reported for the intact system (*60, 85, 87*) with a maximal value of about 1.4.

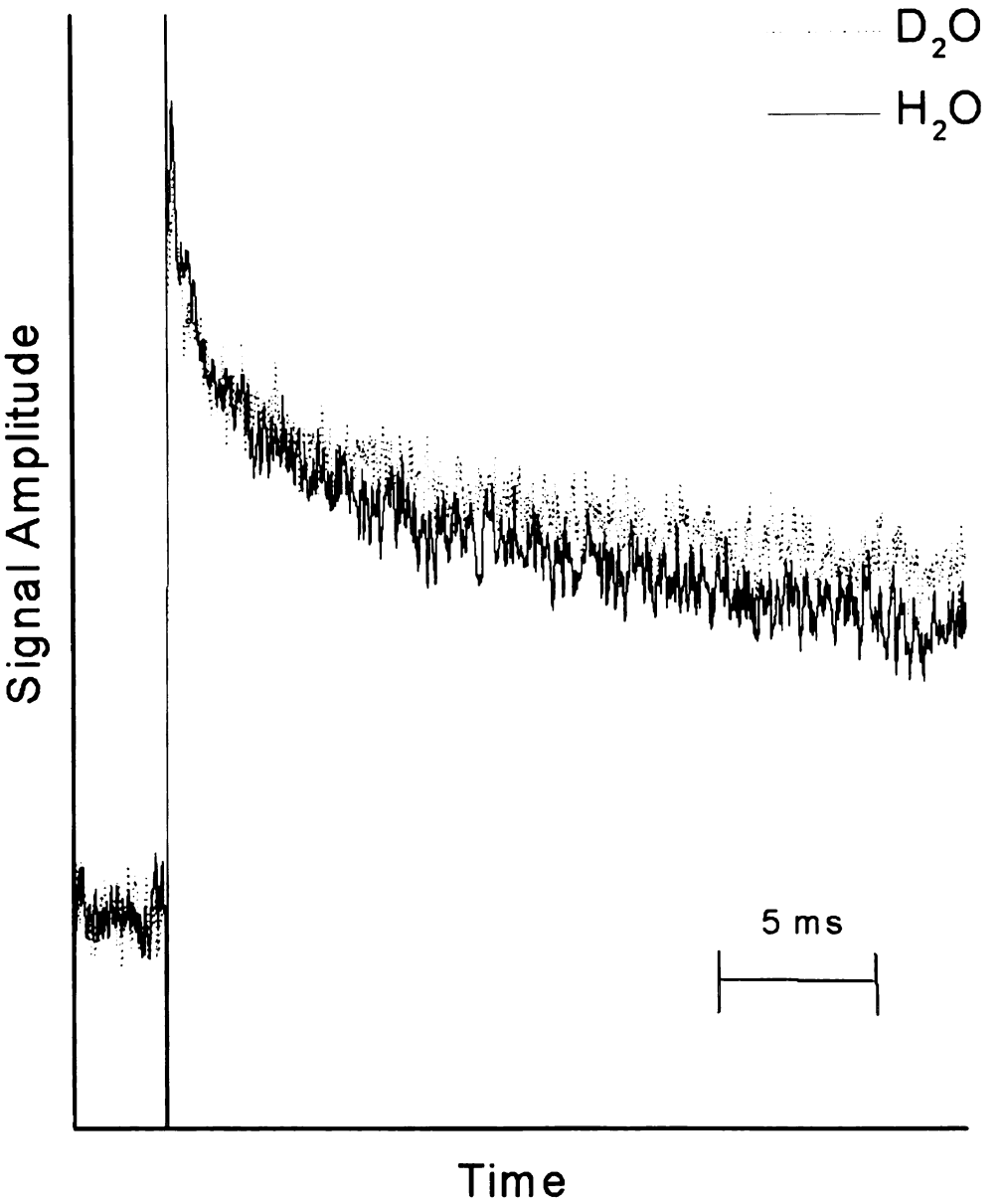

Figure 4-7 Time-resolved EPR steady state kinetic traces (S-states are mixed) for $Y_z^{\bullet}$ reduction in salt-washed PSII membranes reconstituted with $SrCl_2$ in either D_2O or H_2O. The experimental conditions were the same as in Figure 4-2.

Chapter 5

5 Hydrogen Atom Abstraction

5.1 Electron Transfer

The exact function of Ca^{2+} in efficient water oxidation by PSII is currently unknown and was the focus of the time-resolved EPR experiments presented in Chapter 4. The results of these experiments suggest that Ca^{2+} takes on a more generalized role that remains constant throughout the S-state cycle since the kinetics of $Y_z^{\bullet}$ reduction on each S-state transition is retarded by a comparable extent when Ca^{2+} is replaced by Sr^{2+}. Thus, the direct involvement of Ca^{2+} in the oxygen-oxygen bond forming step in water oxidation is unlikely. In addition, similar results have been presented where one or more of the S-state transitions are slowed upon point mutation or biochemical treatment of PSII (Table 1-1). Therefore, in order to show by what mechanism the reduction of $Y_z^{\bullet}$ is altered upon Sr^{2+}-substitution in PSII membranes, we must also take into account the results shown in Table 1-1. To do this, we look at how electron transfer reactions occur, and specifically, how the rates of electron transfer between a donor and acceptor can be affected.

Electron transfer reactions and their rate characteristics have been extensively studied (for a review see (*88*)). Two parts, electronic and nuclear, determine the rate of electron tunneling. The electronic part arises from the dependence on the coupling strength between the electron donor and acceptor wavefunctions; as the distance, R, between donor and acceptor increases, the rate decreases exponentially owing to the uncoupling of the wavefunctions. The

nuclear part depends on the driving force, ΔG, and the reorganization energy, λ. The driving force term is the ground state free energy difference between the donor and acceptor while the reorganization energy is the amount of energy needed to reorganize the nuclear coordinates for electron tunneling. These parameters are defined pictorially in Figure 5-1. A kinetic expression for the estimation of rates of intraprotein, non-adiabatic electron tunneling has been formulated by Page *et al.* (*71*) as follows:

$$\log k_{et} = 13 - ((1.2 - 0.8\rho)(R - 3.6)) - 3.1\ ((\Delta G + \lambda)^2/\lambda]$$

where k_{et} represents the exergonic electron tunneling rate (s^{-1}), ρ is the specific packing density of the inter-cofactor protein volume, R is the edge-to-edge distance between the donor and acceptor (Å), ΔG is the driving force (eV), and λ is the reorganizational energy (eV). We can use this expression to predict the electron transfer rate for the reduction of $Y_z^{\bullet}$ by the Mn cluster to gain a better understanding of the mechanism of this process.

In order to use this kinetic expression for the electron transfer between the Mn cluster and $Y_z^{\bullet}$, we use values to substitute into the equation as follows. The dipolar distance between the Mn cluster and $Y_z^{\bullet}$ has been reported as approximately 8 Å from magnetic-resonance studies (*27-29, 83, 89*). The driving force for this reaction is approximately 60 meV (*90*) and the reorganizational energy is taken to be about 0.8 eV, which is a reasonable estimate for a protein environment (*91-93*). The packing density is determined by the van der Waals

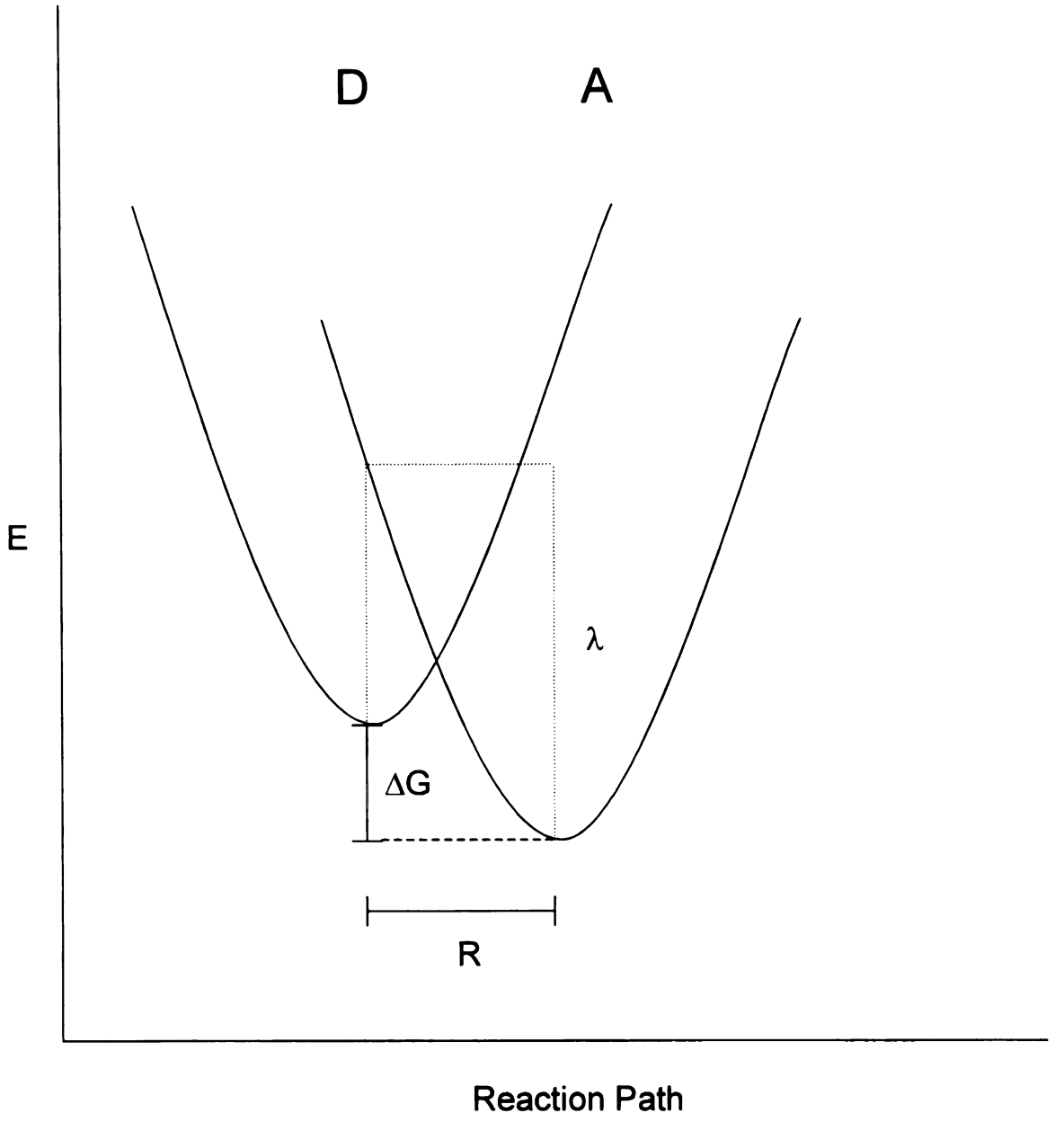

Figure 5-1 Potential energy surfaces of the donor and acceptor. ΔG is the free energy difference between donor and acceptor, λ is the reorganization energy, and R is the distance between donor and acceptor.

radii of the atoms between the donor and acceptor molecules and has an average value of about 0.75 in the proteins analyzed by Page, *et al* (*71*). When these values are substituted into the equation, rates on the ns time scale are predicted, which are orders of magnitude faster than what has been experimentally observed for $Y_z^{\bullet}$ reduction in O_2-evolving systems. Therefore, we conclude that the rate limiting step in the overall $S_n \rightarrow S_{n+1}$ process is not the tunneling of the electron (*71*).

As $Y_z^{\bullet}$ is reduced it becomes protonated (*94, 95*). Thus, a more precise approach to studying this process is within the context of a proton coupled electron transfer (PCET) reaction. We expect that this approach will give additional insight into the rates that we and others (*54, 58, 60, 87*) have measured.

5.2 Proton Coupled Electron Transfer: Sequential or Concerted?

For PCET reactions, three possible mechanistic pathways can be considered, as shown in Figure 5-2. In order to test the viability of each pathway, the energetics of each must be taken into account. The values that were used to determine the energetics of paths a and b are listed in Table 5-1. The first path involves the transfer of the electron, followed sequentially by the transfer of the proton, ET/PT (path a). For the process under investigation here, the transfer of an electron results in the reduction of $Y_z^{\bullet}$ to form the tyrosinate (state II). The reduction potential of $Y^{\bullet}/Y^{-}$ is about 0.68 V aqueous solution (ε = 80) (*96*) and the potential required to oxidize water is about 0.93 V (*8*); therefore the transfer of an electron from substrate water/Mn cluster to $Y_z^{\bullet}$ is an uphill process with a barrier

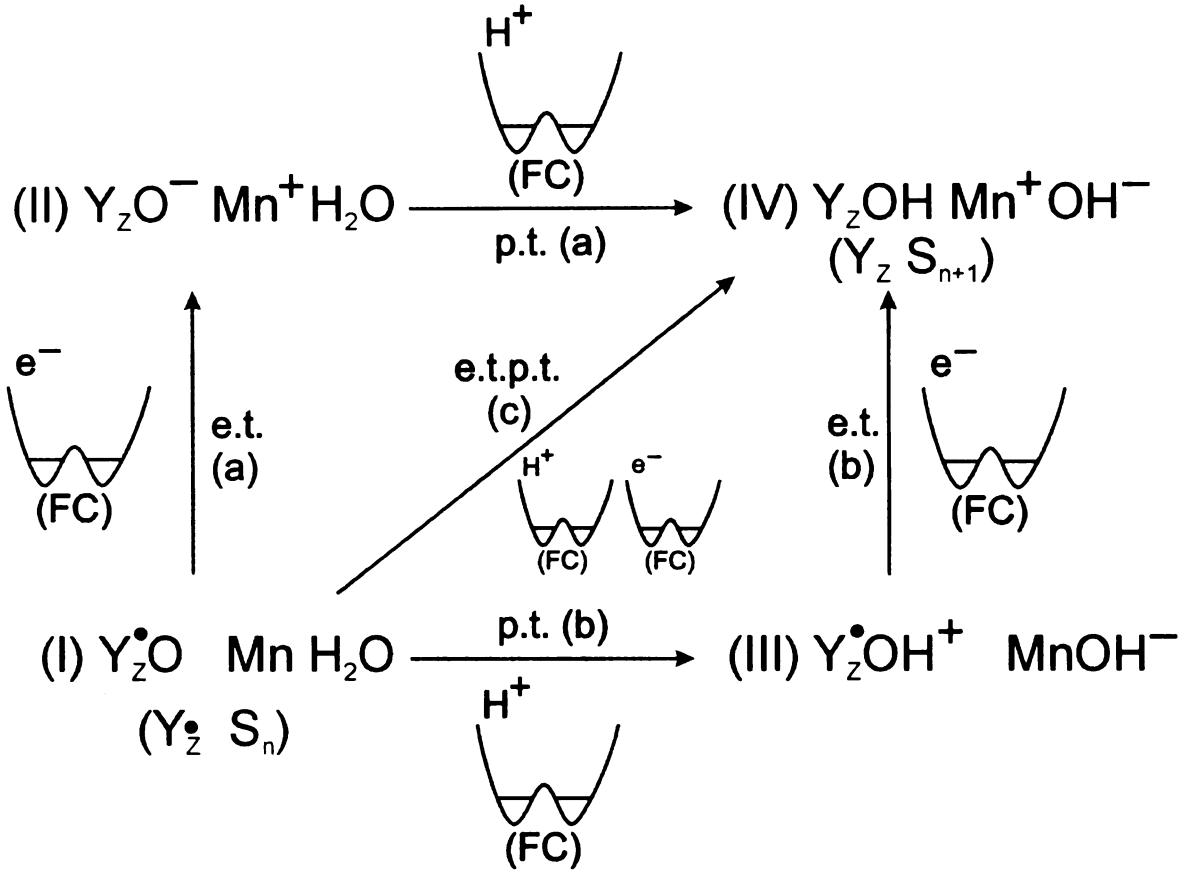

Figure 5-2 Possible reaction paths for proton and electron transfer. The four species that are shown are identified as follows: (I) the reactant state, (IV) the product state, and the two charged intermediate states, (II) and (III). In path (a), electron transfer is followed by proton transfer, while in path (b), proton transfer is followed by electron transfer. In path (c), the electron and proton transfer in a concerted process.

Table 5-1 Reduction Potentials and pK_a Values Used in Determining the Viability of the ET/PT and PT/ET Pathways of Figure 5-1.

Redox couple	Reduction potential	Reference
P_{680}^+/P_{680}	E_m = 1.12 ± 0.05 V	(*6*)
$Y_z^{\bullet}/Y_z$	E_m = 0.97 ± 0.02 V	(*90*)
S_1/S_0	$E_m \leq 0.70$ V	(*90*)
S_2/S_1, S_3/S_2	E_m = 0.90-0.95 V	(*90*)
$Y^{\bullet}/Y^-$	E_m = 0.68 V (aqueous)	(*7*)
O_2/H_2O	E_m = 0.93 V (aqueous)	(*8*)

Molecule	pK_a value	Reference
$Y^{\bullet+}$	-2 (aqueous)	(*7*)
$Mn(H_2O)$	≥ 7	(*38*)

of at least 8 kcal/mol. Furthermore, the difference in reduction potentials between the two cofactors will increase in the low dielectric of a protein environment, resulting in an even larger barrier. We can estimate the effect of the protein dielectric on these potentials by using the Born model:

$$\Delta G = 14.397/\varepsilon r$$

where ΔG (V) is the electrostatic penalty for introducing a charged species with radius r (Å) in a medium with a homogenous dielectric constant ε (*97*). Assuming an average radius of 3 Å for the tyrosine aromatic ring and a dielectric constant of about 8-10, which has been recently suggested for PSII (*98*), the $Y^{\bullet}/Y^{-}$ potential will decrease from an aqueous value of 0.68 V to a value of 0.26 V. This leads to an activation barrier of at least 16 kcal/mol as illustrated in Figure 5-3 (path a), which includes the energy that would be regained from the stabilizing interaction between the positive and negative charge produced. Activation energies have been measured for each of the S-state transitions (see Table 5-2) and are much lower than this estimated barrier. Thus, electron transfer followed by proton transfer is not supported experimentally and this first mechanistic possibility can be discarded.

The second possibility is the transfer of a proton followed by the sequential transfer of an electron, PT/ET, Figure 5-2 (path b). Energetic considerations must also be taken into account to test the viability of forming the cationic tyrosine radical (state III). The pKa's of the proton donor and acceptor

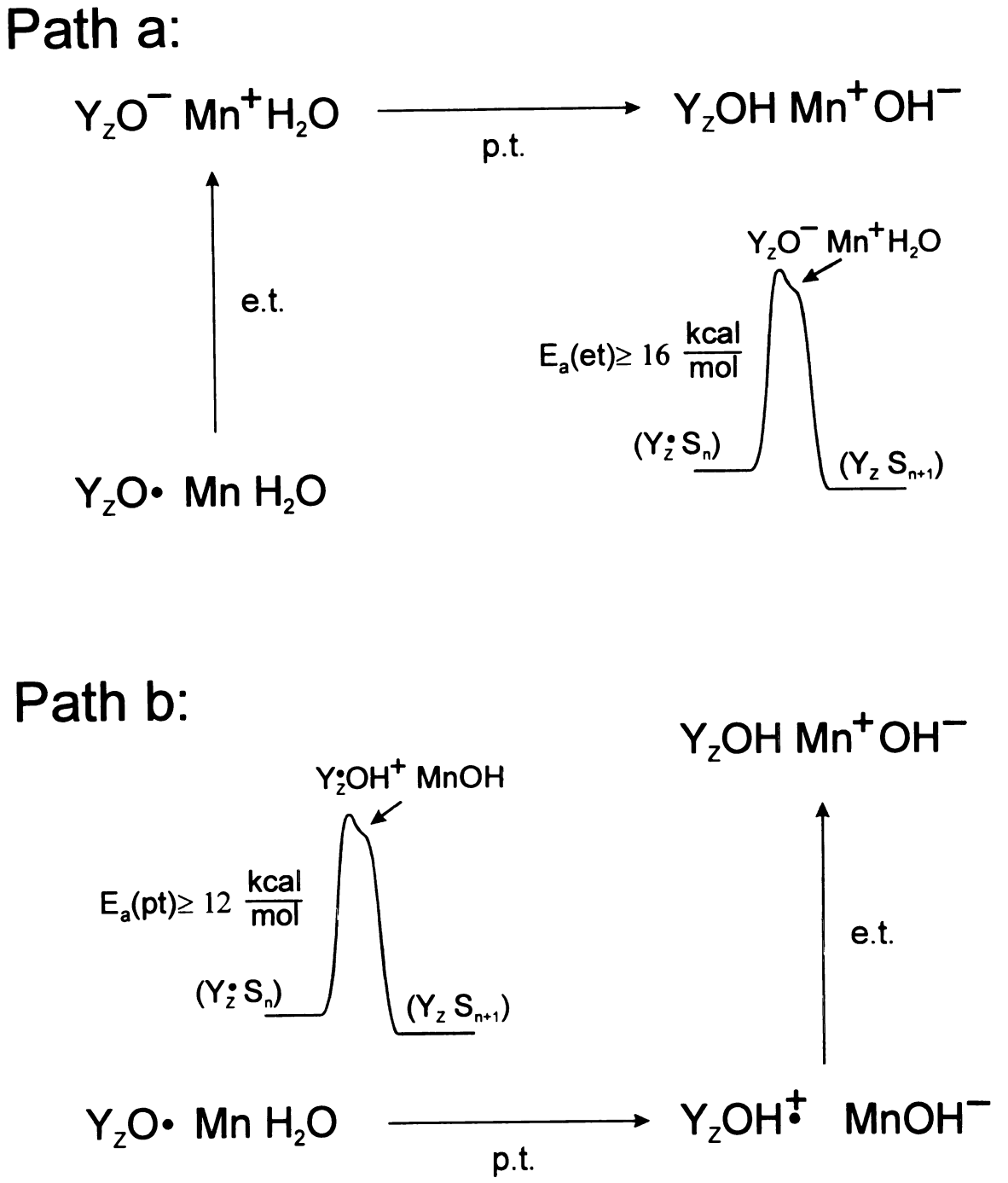

Figure 5-3 Calculated activation energies (E_a) for paths a and b. This figure kindly provided by Gerald T. Babcock.

Table 5-2 Kinetic and Thermodynamic Parameters for the S-state Transitions – Taken from (*7, 59, 60*)

Reaction	E_a (kcal M^{-1})	A (s^{-1})	KIE
$Y_z^{\bullet}S_0 \rightarrow Y_zS_1$	1.2		
$Y_z^{\bullet}S_1 \rightarrow Y_zS_2$	3.0	4.0×10^6	1.3; 2.9
$Y_z^{\bullet}S_2 \rightarrow Y_zS_3$	9.0	5.4×10^9	1.3
$Y_z^{\bullet}S_3 \rightarrow Y_zS_0$	$5.0^{\dagger}$	$8.9 \times 10^{5\dagger}$	1.4-1.6
	$9.2^{\ddagger}$	$2.9 \times 10^{14\ddagger}$	

E_a = activation energy
A = Arrhenius preexponential factor
KIE = kinetic isotope effect

$Y_z^{\bullet}/Y_z$ = reduction potential of $Y_z^{\bullet}/Y_z$
S_{n+1}/S_n = reduction potential of S_{n+1}/S_n

$^{\dagger}T > 280$ K
$^{\ddagger}T < 280$ K

are now important in determining the energetics of the process. The pK_a of a Mn-H_2O complex is expected to be ≥ 7 (*99*), while the pK_a of $Y_z^{\bullet}$ measured in water is –2 (*100*). Thus, the ΔpK_a for the proton transfer is -9, which as Figure 5-3 (path b) illustrates, results in a barrier of at least 12 kcal/mol, with this value reaching greater than 23 kcal/mol in the lower dielectric protein environment. Consequently, the transfer of a proton prior to that of the electron leads to the formation of a barrier at least 3 kcal/mol higher than has been observed for the S-state transitions, which allows us to discard this possibility.

The general characteristics of the S-state transitions are summarized in Table 5-2 and, in many respects, are remarkable. Renger and coworkers have carefully characterized the activation energy E_a and pre-exponential factor *A* for the $S_1 \rightarrow S_2$, $S_2 \rightarrow S_3$, and $S_3 \rightarrow (S_4) \rightarrow S_0$ transitions (*60*). These values are substantially lower than those typically found for an enzyme catalyzed reaction; textbook values are usually taken to be about 10-12 kcal/mol and 10^{13} $M^{-1}s^{-1}$ for E_a and *A*, respectively (*101, 102*). The low *A* values, in particular, are striking. The low rates for $Y_z^{\bullet}$ reduction and the small kinetic isotope effects that have been measured are also unusual considering the small distance between donor and acceptor (*27-29*) and that proton tunneling has been suggested in $Y_z^{\bullet}$ reduction (*59*). Whether the concerted ETPT mechanism can explain these characteristics now becomes the issue at hand.

5.3 Concerted Electron and Proton Transfer

Typical kinetic parameters that are observed for H-atom abstraction by radicals are reported in Tables 5-3 and 5-4. Considering first the E_a values, the

Table 5-3 : Kinetic and Thermodynamic Parameters for H-atom Abstraction Reactions From an Oxygen Atom by an Oxy-based Radical

Reaction	E_a (kcal M^{-1})	log A ($M^{-1}s^{-1}$)	KIE	k ($M^{-1}s^{-1}$)	Ref
4-OMe-Phenol + PhO$^{\bullet}$	n.d.	n.d.	n.d.	4.75×10^5	(*103, 104*)
4-H-Phenol + PhO$^{\bullet}$	4.9[a]	n.d.	n.d.	3.5×10^5	(*103, 104*)
4-*t*-butyl-Phenol + PhO$^{\bullet}$	4.8	5.5	n.d.	51.3	(Mahoney, 1969 #210)
3,5-dimethyl-Phenol + PhO$^{\bullet}$	6.8	6.4	n.d.	16.3	(*104*)
α-tocopherol + PhO$^{\bullet}$	2.0	10.0	1.17	3.1×10^8	(*105*)
α-naphthol + PhO$^{\bullet}$	2.2	8.9	n.d.	2.3×10^7	(*105*)
ubiquinol-0 + PhO$^{\bullet}$	3.5	10.5	n.d.	9.1×10^7	(*105*)
α-tocopherol + $(C_6H_5)_2CO^{\bullet}$	n.d.	n.d.	1.09	5.1×10^9	(Evans, 1992 #217)
α-tocopherol + $(CH_3)_3CO^{\bullet}$	n.d.	n.d.	1.31	3.8×10^9	(Evans, 1992 #217)
$(CH_3)_3CO$-H + $^{\bullet}OC(CH_3)_3$	2.6	6.4	n.d.	n.d.	(*106*)

[a] Calculated by the BEBO method.

Table 5-4: Kinetic and Thermodynamic Parameters for Hydrogen Atom Abstraction by Radicals.

Kinetic and Thermodynamic Parameters for Hydrogen Atom Abstraction by Radicals.

Reaction	E_a (kcal M^{-1})	log *A* ($M^{-1}s^{-1}$)	KIE	k ($M^{-1}s^{-1}$)	Ref
CH_3CH_2-H + $^{\bullet}CH_3$	11.59	11.7	4.04	2.57×10^5	(*107*)
H_3C-H + $^{\bullet}CH_3$	14.51	11.8	3.61	7.41×10^3	(*107*)
SiH_3-H + $^{\bullet}CH_3$	6.98	11.9	3.10	1.20×10^8	(*107*)
NH_2-H + $^{\bullet}CH_3$	9.72	10.8	5.20	2.82×10^5	(*107*)
SH-H + $^{\bullet}CH_3$	2.60	11.6	3.65	1.44×10^{10}	(*107*)
SiH_3-H + $^{\bullet}CH_2CH_3$	7.24	11.7	1.06	5.89×10^7	(*107*)
PhS-H + $^{\bullet}CH_2Ph$	1.5-1.7	9.1-9.4	n.d.	1.3×10^8	(*108*)
$(CH_3)_3Sn$-H + $^{\bullet}CH_3$	3.23	9.4	2.3	1.06×10^7	(*109*)
$(CH_3)_3Sn$-H + $^{\bullet}CH_2CH_3$	3.8	9.1	1.9	2.3×10^6	(*109*)
CH_3CH_2-H + $^{\bullet}OOCH_3$	14.9	11.5	n.d.	n.d.	(*110*)
CH_3-H + $^{\bullet}OOCH_3$	18.48	11.3	n.d.	n.d.	(*110*)

tabulated data span a broad, almost 20 kcal M^{-1} range. However, for reactions in which a hydrogen atom is abstracted from an oxygen atom by an oxy-based radical, which is the situation we postulate in PSII, the situation simplifies and becomes more homogeneous. The E_a values measured for these types of reactions are most often in the range of 2-7 kcal/mol, and are unusually small compared to the values shown in Table 5-4 for other H-atom abstraction reactions, especially those in which C-H or N-H bonds are the hydrogen-atom donor. This phenomenon has been rationalized by Zavitsas and Chatgilialoglu as being due to triplet repulsion in the transition state (TS) (*106*). As the parallel spins on the donor and acceptor molecules move closer together during formation of the TS, a repulsive energy term becomes more significant to the overall activation energy barrier for the reaction. This term is much smaller for H-atom abstraction between $RO^{\bullet}$ and –O-H bonds, thereby allowing the oxygen atoms to form a tighter transition state, which lowers the activation energy barrier. On the other hand, as Table 5-4 shows, H-atom abstraction between two carbon atoms, for example, occurs with much higher activation energies. According to Zavitsas and Chatgilialoglu, this is due to the stronger triplet repulsion experienced by carbon compared to oxygen. In the case of PSII, reduction of $Y_z^{\bullet}$ has been proposed to occur via hydrogen atom abstraction by the tyrosine radical from Mn-ligated water or hydroxide ligands. The low activation energies that have been measured in PSII fit well in this context as reflecting what has been measured in other systems in which H-atom transfer between an oxygen-based radical and an –O-H bond occurs. Other theoretical treatments

have reached similar conclusions with respect to low E_a values, when hydrogen bonding allows relatively close approach of reactant species in a hydrogen-atom transfer process (*81, 124*).

Textbook values for the Arrhenius pre-exponential factor, *A*, for hydrogen-atom abstractions are generally low; $A \cong 10^{8.5}$ $M^{-1}s^{-1}$ is often cited as a typical number (*101, 102*). These values are for second order processes, but with effective PSII concentrations of 1-10 M, the values reported below for first-order PSII processes become essentially directly comparable to the second-order solution reactions. The fact that the S-state transitions also proceed with low *A* factors provides support for our conclusion that the PSII reactions proceed along the concerted pathway in Figure 5-2. We can gain physical insight into the meaning of these values for *A* as follows. The classic interpretation of an *A* factor is as an "attempt frequency". A low *A* value implies an unfavorable entropy of activation, which indicates that the system can position itself to enter the transition state only infrequently. For pure electron tunneling at the short $Y_z^{\bullet}S_n$ distance and for pure proton transfer much higher, typically 10^{13} $M^{-1}s^{-1}$, *A* values are expected (*71, 111*), which indicates a much higher attempt frequency. The fact that these larger *A* values are not found in PSII reinforces our conclusion (*112*) that the sequential pathways, a and b in Figure 5-2, are not likely in the S-state advances.

Figure 5-2 rationalizes the *A*-values in terms of the Franck-Condon (FC) factors for proton and electron transfer and follows closely arguments that have been advanced by Cukier (*113*). A rate constant expression for concerted

PCET can be formulated in analogy to the Marcus-Levich pure ET rate constant as (*114*):

$$k_{etpt} = \frac{V_{el}^2}{\hbar}\sqrt{\frac{\pi}{\lambda_S k_B T}}\sum_{n'}\rho_{in'}\sum_{n}\left|\left\langle \chi_{fn}\middle|\chi_{in'}\right\rangle\right|^2 e^{-(\lambda_S+\Delta G^0+\varepsilon_{fn}-\varepsilon_{in'})^2/4\lambda_S k_B T} \quad (1)$$

The parameters in Eq. (1) that come from the coupling of the reactant and product charge distributions to the surrounding medium are the solvent reorganization (λ_S) and reaction-free energies (ΔG^0); V_{el} is the electronic coupling. These are the standard parameters that determine an ET rate constant's value (*115, 116*). The new ingredients are Franck-Condon factors of the initial (final) state proton vibronic wavefunctions $\chi_{in'}$ (χ_{fn}). The initial states are summed over the equilibrium initial state proton distribution, $\rho_{in'}$. The "effective" activation energy appearing in the exponent of Eq. (1) involves the energetic difference of the proton eigenstates, $\varepsilon_{fn} - \varepsilon_{in'}$, and arises from the requirement of overall energy conservation between the initial and final electron-proton states. The tunneling of the proton is manifested in the Franck-Condon (FC) factors in Eq. (1). These factors tend to be small as they are determined by the overlaps of proton wavefunctions localized around the initial and final proton equilibrium positions, respectively. Thus, concerted PCET is limited by a "Franck-Condon drag" that is a reflection of the requirement that both the electron and the proton are tunneling species. As tunneling is a difficult process, and in concerted PCET there are two tunneling species, the tendency is to obtain relatively small rate constants. However, concerted PCET still can be the dominant reaction channel if the sequential processes are rate limited. As discussed above, both ET/PT

and PT/ET sequential processes are indeed rate limited and that leaves the concerted process as the viable channel. Use of reasonable choices for all the parameters in Eq. (1) does lead to rate-constant values compatible with the magnitudes displayed in Table 2. An important feature of Eq. (1) is that it does not, strictly speaking, have the form $k = A\exp(-E_a / RT)$. Nevertheless, over typical temperature ranges accessible to biological studies, rate constants based on Eq. (1) will approximately obey this form. Thus, we may consider that effective activation energies and pre-exponential factors can be defined for concerted PCET reactions. Evaluation of these factors for appropriate parameter ranges produce values for E_a and A consonant with those in Table 2. In particular, unfavorable entropy of activation factors (low A values) are to be expected for this mechanism. These considerations provide additional support for the notion that the S-state transitions occur by concerted hydrogen-atom transfer.

The rates and kinetic parameters for overall hydrogen-atom transfers can now be rationalized. If the energetics are not too unfavorable, a sequential pathway is more likely, as the Franck-Condon factors do not hinder the reaction appreciably. This appears to be the case in the bacterial reaction center, where the proton-coupled Q_A^- to Q_B^- reaction follows a sequential route (*117*). If, however, the energetics are too unfavorable, as we have argued is the case for the S-state transitions in the OEC, then the concerted pathway is favored. This was also the conclusion drawn by Roth *et al.* (*118*) and by Sjödin et al. (*119*) for their work on small-molecule model compounds. In these two studies, the

authors concluded that the electron transfer/deprotonation process occurred via a concerted mechanism by using similar arguments as those presented above. Thus, for the concerted reaction, the activation energies are generally lower than for the sequential process, but the Franck-Condon drag discussed above lowers the *A* factors and slows the overall rate considerably. The net result is that rates on the order of 10^3-10^5 s^{-1} are observed for both the S-state advances and for $RO^{\bullet} + R'OH \rightarrow ROH + RO'^{\bullet}$ in small organic systems.

In concerted PCET, a substantial isotopic effect can occur, as the deuteron FC factors are smaller than those for a proton. However, these FC factors are strongly dependent on the distance between the flanking heavy atoms that form the hydrogen/deuterium/tritium (H/D/T) bond, with the FC factor increasing for decreasing heavy-atom separation. This increase is more dramatic for T *vs* D *vs* H, and studies conducted by Krishtalik on model compounds have shown that the optimum tunneling distance for H, D, and T are different (*120, 121*). This result leads to the conclusion that it is more favorable for heavier isotopes to spend more energy against the repulsive forces of bringing the flanking atoms together, since tunneling is more difficult than for lighter isotopes. The net result is a decrease in the heavy-atom separation for which tunneling is most effective in the series H, D, T, and this reduces the isotope effect. Furthermore, as the heavy-atom separation decreases, the FC factors saturate to values that are not strongly dependent on distance (*122*). Thus, once the heavy-atom separation is sufficiently small, the distinction between H. D, and T tunnel factors disappears. The rate constants that result

from averaging over the heavy-atom separations then lead to kinetic isotope effects that are much more modest than would otherwise be predicted. Thus, small isotope effects for hydrogen-atom abstractions are expected and are confirmed by theoretical calculations with the result of a proton/deuteron rate ratio of no more than a factor of 2, well in agreement with experimental values of 1.7 and 2.3 reported by the Ingold and Mayer groups, respectively (*105, 118*).

In conclusion, small disturbances of the cluster caused, for example, by the substitution of the larger Sr^{2+} ion, could cause a change in the OEC geometrically and/or electrostatically. Any small change upon the substitution of Sr^{2+}, or any of the other modifications mentioned above, can lead to modification of the activation barrier for hydrogen atom transfer. Since the donor and acceptor species are intimately coupled in these processes, any change that leads to a higher barrier will slow the rate of hydrogen atom transfer. This behavior can explain the reduction in rates seen upon depletion of Ca^{2+} or substitution of Sr^{2+} in the OEC, as well as explain the results of the other modifications to the intact system. For PSII, these effects will be seen on all S-state transitions by causing a slowdown of the reduction of $Y_z^{\bullet}$ by the substrate water/Mn cluster.

BIBLIOGRAPHY

Bibliography

1. Debus, R. J. (1992) *Biochim Biophys Acta 1102*, 269-352.

2. Barber, J., and Kühlbrandt, W. (1999) *Curr. Opin. Struc. Biol. 9*, 469-475.

3. Debus, R. J. (2000) in *Metal Ions in Biological Systems* (Sigel, A., and Sigel, H., Eds.) pp 657-711, Marcel Dekker, Inc., New York.

4. Joliot, P., Barbieri, G., and Chabaud, R. (1969) *Photochem. Photobiol. 10*, 309-329.

5. Kok, B., Forbush, B., and McGolin, M. (1970) *Photochem. Photobiol. 11*, 457-475.

6. Klimov, V. V., Allakhverdiev, S. I., Demeter, S., and Krasnovskii, A. A. (1979) *Dokl. Acad. Nauk. SSSR 249*, 227-230.

7. Tommos, C., and Babcock, G. T. (2000) *Biochim. Biophys. Acta 1458*, 199-219.

8. Krishtalik, L. I. (1986) *Biochim. Biophys. Acta 849*, 162-171.

9. Duysens, L. N. M. (1958) in *Photochemical Apparatus, Brookhaven Symposium in Biology* pp 18, Brookhaven National Laboratory, Upton, NY.

10. Ross, R. T., and Calvin, M. (1967) *Biophys. J. 7*, 595-614.

11. Diner, B. A., and Babcock, G. T. (1996) in *Oxygenic Photosynthesis: The Light Reactions* (Ort, D. R., and Yocum, C. F., Eds.) pp 213-247, Kluwer Academic Publishers, Dordrecht.

12. Yachandra, V. K., Sauer, K., and Klein, M. P. (1996) *Chem. Rev. 96*, 2927-2950.

13. Cinco, R. M., Robblee, J. H., Rompel, A., Fernandez, C., Yachandra, V. K., Sauer, K., and Klein, M. P. (1998) *J. Phys. Chem. 102*, 8248-8256.

14. Zimmermann, J. L., Boussac, A., and Rutherford, A. W. (1986) *Biochemistry 25*, 4609-4615.

15. Zimmermann, J.-L., and Rutherford, A. W. (1984) *Biochim. Biophys. Acta 767*, 160-167.

16. Sivaraja, M., Tso, J., and Dismukes, G. C. (1989) *Biochemistry 28*, 9459-64.

17. Hallahan, B. J., Nugent, J. H. A., Warden, J. T., and Evans, M. C. W. (1992) *Biochemistry 31*, 4562-73.

18. van Vliet, P., Boussac, A., and Rutherford, A. W. (1994) *Biochemistry 33*, 12998-13004.

19. Beck, W. F., de Paula, J. C., and Brudvig, G. W. (1986) *J. Am. Chem. Soc. 108*, 4018-4022.

20. Andreasson, L.-E., Hansson, Ö., and von Schenck, K. (1988) *Biochim. Biophys. Acta 936*, 351-360.

21. Boussac, A., Rutherford, A. W., and Styring, S. (1990) *Biochemistry 29*, 24-32.

22. Haddy, A., Dunham, W. R., Sands, R. H., and Aasa, R. (1992) *Biochim. Biophys. Acta 1099*, 25-34.

23. Casey, J. L., and Sauer, K. (1984) *Biochim. Biophys. Acta 767*, 21-28.

24. Boussac, A., Zimmermann, J.-L., Rutherford, A. W., and Lavergne, J. (1990) *Nature 347*, 303-306.

25. Gilchrist, M. L., Jr., Ball, J. A., Randall, D. W., and Britt, R. D. (1995) *Proc. Natl. Acad. Sci. U.S.A. 92*, 9545-9549.

26. Tang, X. S., Randall, D. W., Force, D. A., Diner, B. A., and Britt, R. D. (1996) *J. Am. Chem. Soc. 118*, 7638-7639.

27. Dorlet, P., Di Valentin, M., Babcock, G. T., and McCracken, J. L. (1998) *J. Phys. Chem. B 102*, 8239-8247.

28. Peloquin, J. M., Campbell, K. A., and Britt, R. D. (1998) *J. Am. Chem. Soc. 120*, 6840-6841.

29. Lakshmi, K. V., Eaton, S. S., Eaton, G. R., Frank, H. A., and Brudvig, G. W. (1998) *J. Phys. Chem. B 102*, 8327-8335.

30. Ono, T.-a., Noguchi, T., Inoue, Y., Kusunoki, M., Matsushita, T., and Oyanagi, H. (1992) *Science 258*, 1335-1337.

31. Roelofs, T. A., Liang, W. C., Latimer, M. J., Cinco, R. M., Rompel, A., Andrews, J. C., Sauer, K., Yachandra, V. K., and Klein, M. P. (1996) *Proc. Natl. Acad. Sci. USA 93*, 3335-3340.

32. Iuzzolino, L., Dittmer, J., Dorner, W., Meyer-Klaucke, W., and Dau, H. (1998) *Biochemistry 37*, 17112-17119.

33. Barry, B. A., and Babcock, G. T. (1987) *Proc. Nat. Acad. Sci, USA 84*, 7099-7103.

34. Diner, B. A., Force, D. A., Randall, D. W., and Britt, R. D. (1998) *Biochemistry 37*, 17931-17943.

35. Blankenship, R. E., Babcock, G. T., Warden, J. T., and Sauer, K. (1975) *FEBS Lett. 51*, 287-293.

36. Warden, J. T., Blankenship, R. E., and Sauer, K. (1976) *Biochim. Biophys. Acta 423*, 462-478.

37. Hoganson, C. W., and Babcock, G. T. (1997) *Science 277*, 1953-1956.

38. Tommos, C., and Babcock, G. T. (1998) *Accounts Chem. Res. 31*, 18-25.

39. Babcock, G. T. (1995) in *Photosynthesis: from Light to Biosphere* (Mathis, P., Ed.) pp 209-215, Kluwer Academic Publishers, Netherlands.

40. Hoganson, C. W., Lydakis-Simantiris, N., Tang, X.-S., Tommos, C., Warncke, K., Babcock, G. T., Diner, B. A., McCracken, J., and Styring, S. (1995) *Photosynthesis Res. 46*, 177-184.

41. Brettel, K., Schlodder, E., and Witt, H. T. (1984) *Biochim. Biophys. Acta 766*, 403-415.

42. Meyer, B., Schlodder, E., Dekker, J. P., and Witt, H. T. (1989) *Biochim. Biophys. Acta 974*, 36-43.

43. Rappaport, F., and Lavergne, J. (1997) *Biochemistry 36*, 15294-15302.

44. Schilstra, M. J., Rappaport, F., Nugent, J. H. A., Barnett, C. J., and Klug, D. R. (1998) *Biochemistry 37*, 3974-3981.

45. Christen, G., and Renger, G. (1999) *Biochemistry 38*, 2068-2077.

46. Christen, G., Seeliger, A., and Renger, G. (1999) *Biochemistry 38*, 6082-6092.

47. Hays, A.-M., Vassiliev, I. R., Golbeck, J. H., and Debus, R. J. (1999) *Biochemistry 38*, 11851-11865.

48. Diner, B. A., Nixon, P. J., and Farchaus, J. W. (1991) *Curr. Opin. Struct. Biol. 1*, 546-554.

49. Roffey, R. A., Kramer, D. M., Govindjee, and Sayre, R. T. (1994) *Biochim. Biophys. Acta 1185*, 257-270.

50. Chu, H.-A., Nguyen, A. P., and Debus, R. J. (1995) *Biochemistry 34*, 5839-5858.

51. Hays, A. M. A., Vassiliev, I. R., Golbeck, J. H., and Debus, R. J. (1998) *Biochemistry 37*, 11352-11365.

52. Mamedov, F., Sayer, R. T., and Styring, S. (1998) *Biochemistry 37*, 14245-14256.

53. Babcock, G. T., Blankenship, R. E., and Sauer, K. (1976) *FEBS Lett. 61*, 286-289.

54. Razeghifard, M. R., Klughammer, C., and Pace, R. J. (1997) *Biochemistry 36*, 86-92.

55. Dekker, J. P., Demetrios, F. G., Plijter, J. J., Van Gorkon, H. J., and Babcock, G. T. (1984) *Biochim. Biophys. Acta 767*, 515-523.

56. Boussac, A., Setif, P., and Rutherford, A. W. (1992) *Biochemistry 31*, 1224-34.

57. Razeghifard, M. R., Wydrzynski, T., Pace, R. J., and Burnap, R. L. (1997) *Biochemistry 36*, 14474-8.

58. Razeghifard, M. R., and Pace, R. J. (1997) *Biochim. Biophys. Acta 1322*, 141-150.

59. Tommos, C., Hoganson, C. W., Di Valentin, M., Lydakis-Simantiris, N., Dorlet, P., Westphal, K., Chu, H.-A., McCracken, J., and Babcock, G. T. (1998) *Curr. Opin. Chem. Biol. 2*, 244-252.

60. Karge, M., Irrgang, K. D., and Renger, G. (1997) *Biochemistry 36*, 8904-8913.

61. Hundelt, M., Hays, A.-M., Debus, R. J., and W., J. (1998) *Biochemistry 37*, 14450-14456.

62. Ghanotakis, D. F., Babcock, G. T., and Yocum, C. F. (1984) *FEBS Lett. 167*, 127-130.

63. Boussac, A., and Rutherford, A. W. (1988) *Biochemistry 27*, 3476-3483.

64. Boussac, A., and Rutherford, A. W. (1988) *Chem. Scripta 28A*, 123-126.

65. Latimer, M. J., Derose, V. J., Mukerji, I., Yachandra, V. K., Sauer, K., and Klein, M. P. (1995) *Biochemistry 34*, 10898-10909.

66. Noguchi, T., Ono, T., and Inoue, Y. (1995) *Biochimica Et Biophysica Acta-Bioenergetics 1228*, 189-200.

67. Pecoraro, V. L., Baldwin, M. J., Caudle, M. T., Hsieh, W.-Y., and Law, N. A. (1998) *Pure & Appl. Chem. 70*, 925-929.

68. Siegbahn, P. E. M., and Crabtree, R. H. (1999) *J. Am. Chem. Soc. 121*, 117-127.

69. Limburg, J., Vrettos, J. S., Liable-Sands, L. M., Rheingold, A. L., Crabtree, R. H., and Brudvig, G. W. (1999) *Science 283*, 1524-1527.

70. Limburg, J., Szalai, V. A., and Brudvig, G. W. (1999) *J. Chem. Soc., Dalton Trans. 9*, 1353-1361.

71. Page, C. C., Moser, C. C., Chen, X., and Dutton, P. L. (1999) *Nature 402*, 47-52.

72. Riggs-Gelasco, P. J., Mei, R., Ghanotakis, D. F., Yocum, C. F., and Penner-Hahn, J. E. (1996) *J. Am. Chem. Soc. 118*, 2400-2410.

73. Scheiner, S. (1994) *Acc. Che. Res. 27*, 402-408.

74. Berthold, D. A., Babcock, G.T., and Yocum, C.F. (1981) *FEBS Lett. 134*, 231-234.

75. Ghanotakis, D. F., Demetriou, D. M., and Yocum, C. F. (1987) *Biochim. Biophys. Acta 891*, 15-21.

76. Ghanotakis, D. F., Topper, J., Babcock, G. T., and Yocum, C. F. (1984) *Biochim. Biophys. Acta 767*, 524-531.

77. Hillier, W., Messinger, J., and Wydrzynski, T. (1998) *Biochemistry 37*, 16908-16914.

78. Tommos, C., McCracken, J., Styring, S., and Babcock, G. T. (1998) *J. Am. Chem. Soc. 120*, 10441-10452.

79. Qian, M., Dao, L. A., Debus, R. J., and Burnap, R. L. (1999) *Biochemistry 38*, 6070-6081.

80. Hillier, W., and Wydrzynski, T. (2000) *Biochemistry in press*.

81. Hoganson, C. W., and Babcock, G. T. (1988) *Biochemistry 27*, 5848-5855.

82. Babcock, G. T. (1987) in *New Comprehensive Biochemistry* (Amesz, J., Ed.) pp 125-158, Elsevier, Amsterdam.

83. Lakshmi, K. V., Eaton, S. S., Eaton, G. R., and Brudvig, G. W. (1999) *Biochemistry 38*, 12758-12767.

84. Rappaport, F., Blanchard-Desce, M., and Lavergne, J. (1994) *Biochim. Biophys. Acta 1184*, 178-192.

85. Lydakis-Simantiris, N., Ghanotakis, D. F., and Babcock, G. T. (1997) *Biochim. Biophys. Acta. 1322*, 129-140.

86. Cha, Y., Murray, C.J., & Klinman, J.P. (1989) *Science 243*, 1325-1330.

87. Haumann, M., Bogershausen, O., Cherepanov, D., Ahlbrink, R., and Junge, W. (1997) *Photosynth. Res. 51*, 193-208.

88. Barbara, P. F., Meyer, T. J., and Ratner, M. A. (1996) *Journal of Physical Chemistry 100*, 13148-13168.

89. MacLachlan, D. J., Nugent, J. H. A., Warden, J. T., and Evans, M. C. W. (1994) *Biochim. Biophys. Acta 1188*, 325-334.

90. Vass, I., and Styring, S. (1991) *Biochemistry 30*, 830-839.

91. Winkler, J. R., and Gray, H. B. (1992) *Chemical Reviews 92*, 369-379.

92. McLendon, G., and Hake, R. (1992) *Chemical Reviews 92*, 481-490.

93. Moser, C. C., Keske, J. M., Warncke, K., Farid, R. S., and Dutton, P. L. (1992) *Nature 355*, 796-802.

94. Un, S., Tang, X.-S., and Diner, B. A. (1996) *Biochemistry 35*, 679-684.

95. Berthomieu, C., Hienerwadel, R., Boussac, A., Breton, J., and Diner, B.A. (1998) *Biochemistry 37*, 10547-10554.

96. Clark, W. M. (1960) *Oxidation-Reduction Potentials of Organic Systems*, The Williams & Wilkins Company, Baltimore, VA.

97. Rich, P. R., Meunier, B., Mitchell, R., and Moody, A. J. (1996) *Biochim. Biophys. Acta 1275*, 91-95.

98. Mulkidjanian, A. Y. (1999) *Biochim. Biophys. Acta 1410*, 1-6.

99. Caudle, M. T., and Pecoraro, V. L. (1997) *J. Am. Chem. Soc. 119*, 3415-3416.

100. Dixen, W. T., and Murphy, D. (1976) *J. Chem. Soc. Faraday Trans. II 72*, 1221-1230.

101. Segel, I. H. (1975) *Enzyme Kinetics, Behavior and Analysis of Rapid Equilibrium and Steady-State Enzyme Systems*, John Wiley & Sons, New York.

102. Chance, B., DeVault, D. C., Frauenfelder, H., Marcus, R. A., Schrieffer, J. R., and Sutin, N. (1979) *Tunneling in Biological Systems*, Academic Press, New York.

103. Mahoney, L. R., and DaRooge, M. A. (1975) *J. Am. Chem. Soc. 97*, 4722-4731.

104. Mahoney, L. R., and DaRooge, M. A. (1972) *J. Am. Chem. Soc. 94*, 7002-7009.

105. Foti, M., Ingold, K. U., and Lusztyk, J. (1994) *J. Am. Chem. Soc. 116*, 9440-9447.

106. Zavitsas, A. A., and Chatgilialoglu, C. (1995) *J. Am. Chem. Soc. 117*, 10645-10654.

107. Arthur, N. L., and Bell, T. N. (1978) *Rev. Chem. Intermed. 2*, 37-74.

108. Franz, J. A., Bushaw, B. A., and Alnajjar, M. S. (1989) *J. Am. Chem. Soc. 111*, 268-275.

109. Chatgilialoglu, C., Ingold, K. U., and Scaiano, J. C. (1981) *J. Am. Chem. Soc. 103*, 7739-7742.

110. Mims, C. A., Mauti, R., Dean, A. M., and Rose, K. D. (1994) *J. Phys. Chem. 98*, 13357-13372.

111. Silverman, D. N. (2000) *Biochim. Biophys. Acta 1458*, 88-103.

112. Westphal, K. L., Tommos, C., Cukier, R. I., and Babcock, G. T. (2000) *Current Opinions in Plant Biology 3*, 236-242.

113. Cukier, R. I. (1999) *J. Phys. Chem. A 103*, 5989-5995.

114. Cukier, R. I., and Nocera, D. G. (1998) *Annu. Rev. Phys. Chem. 49*, 337-369.

115. Ulstrup, J. (1979) *Charge Transfer Processes in Condensed Media*, Springer, Berlin.

116. Marcus, R. A., and Sutin, N. (1985) *Biochim. Biophys. Acta 811*, 265.

117. Okamura, M. Y., Paddock, M. L., Graige, M. S., and Feher, G. (2000) *in press*.

118. Roth, J. P., Lovell, S., and Mayer, J. M. (2000) *J. Am. Chem. Soc. ASAP*.

119. Sjodin, M., Stenbjorn, S., Akermark, B., Sun, L., and Hammarstrom, L. (2000) *J. Am. Chem. Soc. 122*, 3932-3935.

120. Krishtalik, L. I. (2000) *Biochim. Biophys. Acta 1458*, 6-27.

121. Krishtalik, L. I. (1979) *J. Electroanalyt. Chem. 100*, 547-561.

122. Cukier, R. I., and Zhu, J. (1997) *J. Phys. Chem. 101*, 7180-7188.